UNIVERSITY OF CALIFORNIA
RIVERSIDE

Spin and Valley Physics in Two Dimensional Systems: Graphene and Superconducting Transition Metal Dichalcogenides

A Dissertation submitted in partial satisfaction
of the requirements for the degree of

Doctor of Philosophy

in

Physics

by

Evan Boyd Sosenko

August 2016

Dissertation Committee:

Dr. Vivek Aji, Chairperson
Dr. Nathaniel Gabor
Dr. Leonid Pryadko

The Dissertation of Evan Boyd Sosenko is approved:

Committee Chairperson

University of California, Riverside

Acknowledgments

I wish to express my immense gratitude to my adviser Dr. Vivek Aji, who guided my work, but always left space to solve things my own way. I am truly fortunate to have found a passionate and amiable adviser. He always has an answer to my questions (with corresponding references), and is quickly able to pick out the critical physics needed to carry on whenever I get stuck.

Deep thanks to my committee members, Dr. Nathaniel Gabor and Dr. Leonid Pryadko, and my qualifying exam committee members, Dr. Shan-Wen Tsai and Dr. Gregory Beran, for supporting, questioning, and helping me realize the wider impact of my research. This work would not be possible without the strong collaboration of our research group members, Dr. Huazhou Wei, Michael Phillips, and Dr. Junhua Zhang.

Thanks to my undergraduate institution, the College of Creative Studies at the University of California, Santa Barbara, for forging my beginnings as a physicist and granting me the Regents Scholarship. Thank you to the University of California, Riverside, for supporting my work though the Chancellor's Distinguished Fellowship Award, Dr. Umar Mohideen, for heading and growing our physics department, and Derek Beving, for navigating me though any administrative mazes.

The text of this thesis, in part or in full, is a reprint of the material as it appears in Physical Review B [1] and a manuscript, pending publication with the American Physical Society, which is currently available as an e-print on the arXiv [2]. The co-author, Dr. Vivek Aji, listed in those publications directed and supervised the research which forms the basis for this thesis. The software developed and used [3] for this work and the included figures is available freely online.[1] We acknowledge

[1] Related software and source code at `https://evansosenko.com/spin-lifetime` and `https://evansosenko.com/dichalcogenides`

useful discussions with Adrian Swartz, Sung-Po Chao, and Roland Kawakami, who made his research data available for general use. We recognize the support of a UCR Senate Research Grant, two GSA Conference Travel Grants, and the Army Research Office through the grant ARO W911NF1510079.

Finally, I would like to thank my fellow grads, friends, family, and parents for their unwaivering and positive support of my intellectual pursuits.

To my parents John and Jennifer, whose love and support is absolute,

and to Anita Boyd, my grandmother and first teacher.

Abstract of the Dissertation

Spin and Valley Physics in Two Dimensional Systems:
Graphene and Superconducting Transition Metal Dichalcogenides

by

Evan Boyd Sosenko

Doctor of Philosophy, Graduate Program in Physics
University of California, Riverside, August 2016
Dr. Vivek Aji, Chairperson

Recent focus on two dimensional materials and spin-coupled phenomena holds future potential for fast, efficient, flexible, and transparent devices.

The fundamental operation of a spintronic device depends on the injection, transmission, and detection of spins in a conducting channel. Long spin lifetimes during transit are critical for realizing this technology. An attractive platform for this purpose is graphene, which has high mobilities and low spin-orbit coupling. Unfortunately, measured spin lifetimes are orders of magnitude smaller than theoretically expected. A source of spin loss is the resistance mismatch between the ferromagnetic electrodes and graphene. While this has been studied numerically, here we provide a closed form expression for Hanle spin precession which is the standard method of measuring spin lifetimes. This allows for a detailed characterization of the nonlocal spin valve device.

Strong spin-orbit interaction has the potential to engender unconventional superconducting states. A cousin to graphene, two dimensional transition metal dichalcogenides entwine interaction, spin-orbit coupling, and topology. The noninteracting electronic states have multiple valleys in the energy dispersion and are topologically

nontrivial. We report on the possible superconducting states of hole-doped systems, and analyze to what extent the correlated phase inherits the topological aspects of the parent crystal. We find that local attractive interactions or proximal coupling to s-wave superconductors lead to a pairing which is an equal mixture of a spin singlet and the $m = 0$ spin triplet. Its topology allows quasiparticle excitations of net nonzero Berry curvature via pair-breaking by circularly polarized light. The valley contrasting optical response, where oppositely circularly polarized light couples to different valleys, is present even in the superconducting state, though with smaller magnitude.

Contents

List of Figures

Chapter 1

Introduction

The discovery of single-atomic-layer graphene in 2004 inspired a new generation of research on two-dimensional semiconductors [4]. These 2D materials display extraordinary properties not present in the bulk. Graphene boasts high electron mobility and exceptional strength. Single-layer transition metal group-VI dichalcogenides (TMDs) exhibit spin-coupled optoelectronic properties and a new valley degree of freedom. Monolayers are inherently flexible and transparent, and future devices fabricated from 2D layers promise novel applications, reduced size, and lower power requirements.

A relatively new field, breakthroughs in spintronics have already impacted the tech industry. In 2007, Albert Fert and Peter Grünberg were awarded the Nobel prize in Physics for the discovery of Giant magnetoresistance (GMR) which found wide application in computer storage technology [5]. The potential applications of 2D materials for building new spintronic devices is equally exciting. Such devices would encode signals in spin current as opposed to electric current.

Building a dynamic spin transport device using a spin degenerate material like graphene relies on some external means to polarize the spin. Typically, electrons are

forced though a ferromagnetic contact which polarizes the spin along a single axis. Any viable material must be a good conductor of spin current. As spin polarized electrons travel through a conducting channel, internal scattering events which flip spin tend to randomize the signal. The spin lifetime is the characteristic timescale over which this signal will survive, and thus it determines the length scale for a realistic device. Finding a material with suitably long spin lifetimes is critical for realizing any spin transport device. While theoretical predictions for graphene suggest microsecond lifetimes, experimental measurements report lifetimes six orders of magnitude less.

Chapter 2 of this thesis concerns the discrepancy between the theoretically predicted spin lifetimes in graphene and the significantly longer experimentally measured ones. We present an analytical solution to the drift-diffusion equation modeling a canonical nonlocal spin value experiment which includes the effects of the ferromagnetic contacts. The device, shown in figure 1.1, is subject to a varying magnetic field, and the resulting Hanle curve generated by measuring the spin signal is used to extract the effective spin lifetime. Using real data, we then analyze the reliability of fitting this model over critical parameter regimes, particularly in the case of large lifetimes.

Another excellent candidate for spintronic devices, TMDs are materials with strong spin-orbit coupling that break spin degeneracy and provide an intrinsic means to control the spin signal. In particular, TMDs show a strong coupling between polarized light and their valley degree of freedom. Since each band is spin-split, controlled optical excitations may selectively activate carriers of a single valley and spin population. Additionally, each valley has opposite Berry curvature, so electrons in different valleys drift in opposite directions transverse to an applied in-plane electric field.

Chapter 3 of this thesis characterizes the possible superconducting phases for

monolayer TMDs in a regime where the spin and valley degrees of freedom are locked. We consider phases arising from proximity to a normal superconductor or effective attractive electron-electron interactions. The valley selective optical excitation rules and topological character are reproduced in the context of the superconducting state.

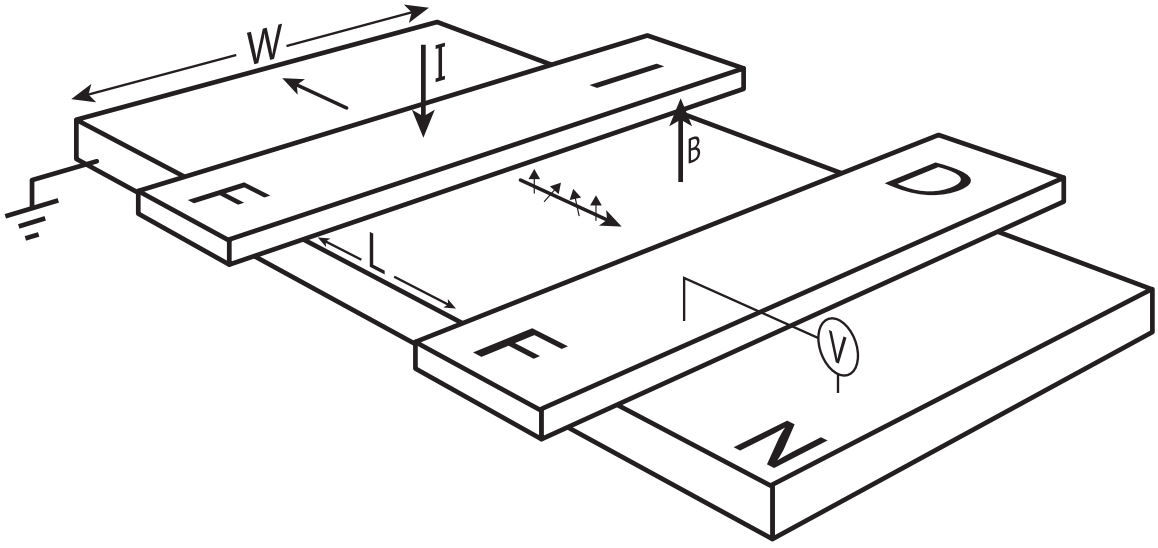

Figure 1.1: Isometric representation of a nonlocal spin valve in a magnetic field. Current is injected into the semiconductor through the left ferromagnetic contact. The strength of the diffusive spin signal is measured as a voltage at the right ferromagnetic contact.

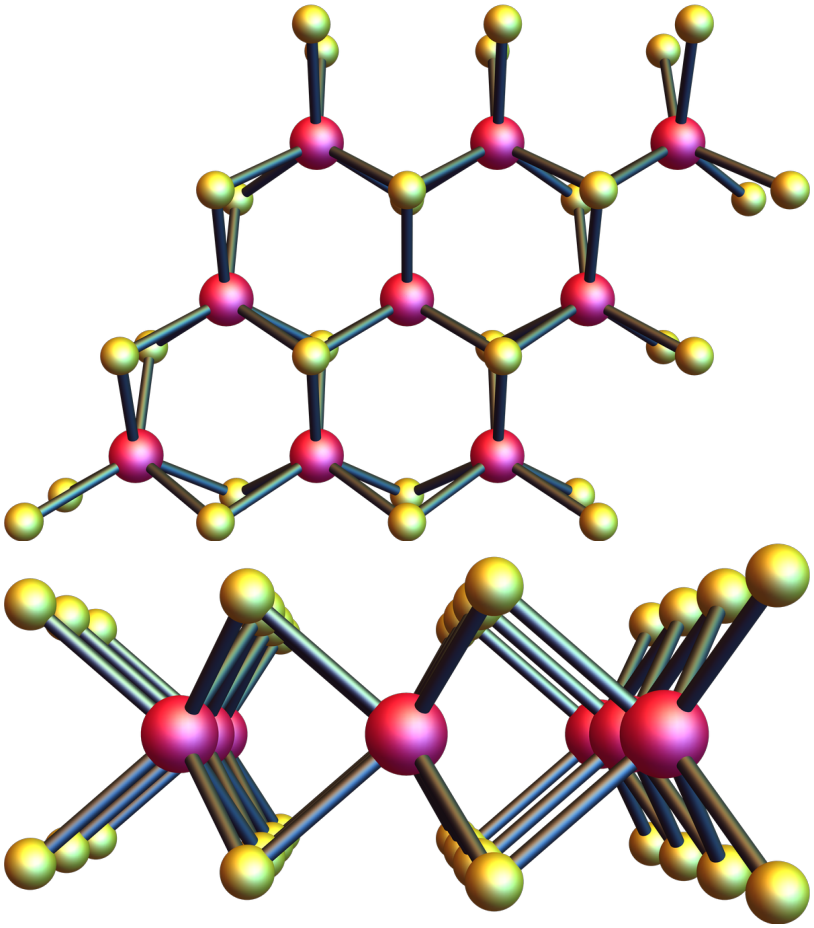

Figure 1.2: Top and side views of the crystal structure of monolayer MoS_2.

Chapter 2

Spin Lifetime

2.1 Introduction

Spintronic devices rely on the ability to inject, transport, manipulate, and detect spins [6, 7]. The typical architecture involves ferromagnetic electrodes deposited on a conducting medium [8, 9]. Driving a current across the junction of a magnetic element and a nonmagnetic metal leads to spin injection (also called spin accumulation) [9–12]. The injected spins either diffuse in nonlocal spin valve geometry, or are driven by applied fields across the conducting channel. The former has the advantage that the observed spin signal is not corrupted by accompanying charge current. During this transit, scattering processes dephase the spins and thus degrade the chemical potential imbalance between spins of opposite orientation. The residual difference is detected by a ferromagnetic electrode whose magnetization can be flipped by applying external fields.

The performance of devices is determined by a number of parameters associated with the basic processes described above. The efficiency of spin injection, the dif-

fusion length (or equivalently the diffusion constant and spin relaxation time), the distance between the injector and detector, and resistivities of various components such as the electrodes, the junction, and the conducting channel, are some of the ingredients that contribute to the measured magnetoresistance. As such, having good injection efficiency coupled with long spin lifetimes is crucial for the viability of spintronic applications. The discovery of graphene [13] has been of particular interest in this regard because of its tunable conductivity, high mobility, and low spin-orbit coupling. Moreover, the two dimensional nature allows for efficient device design and spin manipulation. Theoretical estimates for spin lifetimes of a few microseconds [14, 15] are leading to a concerted effort in realizing spin based transistors and spin valves [16–23].

Unfortunately, the best measured spin lifetimes via the Hanle spin precession technique are in the 50 ps to 200 ps range [16, 23–25]. The large discrepancy is yet to be explained. The linear scaling of spin and transport lifetimes [23] suggested that the dominant scattering mechanism in the conducting channeling is of the Elliot-Yafet type [26]. Surprisingly, in the regime of small spin lifetimes ($\sim$ 100 ps), Coulomb scattering was shown not to be the dominant mechanism [25]. The more important determining factor of the lifetime was found to be the nature of the interface between the magnetic electrode and the conducting channel. Tunneling contacts suppress spin relaxation, and lifetimes of 771 ps were reported at room temperature, increasing to 1.2 ns at 4 K [27]. On the other hand, low resistance barriers lead to considerable uncertainty in the determination of the lifetimes.

Over the last few years, characterizing the nature of the spin dynamics at the interface has garnered much attention. A key contribution in this effort is the generalization of the standard theoretical approach of calculating the nonlocal magne-

toresistance with and without the magnetic field. Recent efforts study the effect of including the contact resistance [24, 28], and alternatively relaxing the normally infinite boundary conditions in favor of a finite channel size [29]. The approach relies on numerically solving the Bloch equation to generate Hanle precession curves and then fitting observed data.

In this chapter, we present the closed form expression for the precession curves with finite contact resistance, and analytically discuss the various parameters regimes that show qualitatively different behaviors. The fits to data reproduce the results in the literature and provide a means to understand the effect of the contacts which were previously obtained by numerical simulations.

This chapter is organized as follows. In section 2.2 we provide the basic model, define the relevant parameters, and present an expression for the nonlocal resistance R_{NL}. The primary result is given by equation (2.4). In section 2.3 the solution for R_{NL} is fitted to data. In section 2.4 we analyze the various regimes which are determined by the diffusion length, length of the device, and the contact resistance.

2.2 Model

The assumed device geometry is shown in figure 2.1. Two ferromagnetic contacts (F) are deposited on the normal semiconductor (N). A spin-polarized current I is injected through the contact at $x = 0$ and flows in the $x \leq 0$ region of the semiconductor. The voltage difference V is measured at $x = L$ between the contact and the semiconductor. The nonlocal resistance is $R_{\mathrm{NL}} = V/I$ [28].

Spin transport is modeled by identifying two spin channels and their associated three-component spin electrochemical potentials $\mu_{\uparrow\downarrow}$. The majority channel is labeled

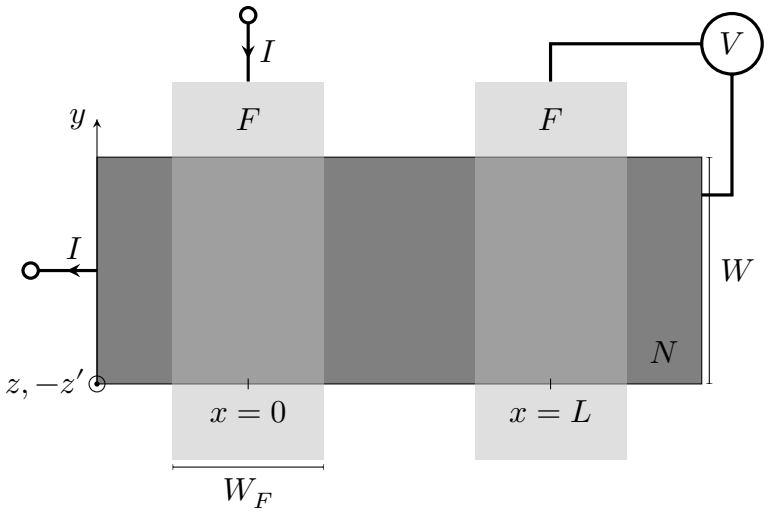

Figure 2.1: The geometry of the nonlocal spin valve analyzed in this chapter is shown. There are two ferromagnetic electrodes placed on a conducting channel. Current I flows into the left electrode, while the potential V is measured at the right electrode. The nonlocal resistance is defined as the ratio V/I. For spin dependent phenomena, the relevant quantity of interest is the difference between the nonlocal resistance for the parallel and antiparallel orientations of magnetization of the two electrodes.

as up, while the minority channel is labeled as down. The voltage difference is proportional to the spin accumulation $\mu_s = \left(\mu_\uparrow - \mu_\downarrow\right)/2$ at $x = L$. The spin accumulation in the semiconductor is assumed to satisfy the steady-state Bloch diffusion equation

$$D\nabla^2\mu_s^N - \frac{\mu_s^N}{\tau} + \omega \times \mu_s^N = 0. \tag{2.1}$$

The key parameters are the contact spacing L, the diffusion constant D, the spin lifetime τ, the spin diffusion length $\lambda = \sqrt{D\tau}$, and $\omega = (g\mu_B/\hbar)\, B$ which is proportional to the applied magnetic field B and the gyromagnetic ratio $g = 2$.

For contacts which cover the width of the channel, the transport is uniform along y. Since the channel is two-dimensional, μ_s^N will only vary along x. We enforce the boundary condition $\mu_s^N \to 0$ at $x \to \pm\infty$ and the continuity of the current and spin

current. A detailed derivation is given in appendix A and reveals

$$R_{\mathrm{NL}}^{\pm} = \pm p_1 p_2 R_N f. \tag{2.2}$$

The overall sign corresponds to parallel and antiparallel ferromagnetic alignments. Specifically, we find a resistance scale

$$R_N = \frac{\lambda}{WL}\frac{1}{\sigma^N}, \tag{2.3}$$

and the function

$$f = \mathrm{Re}\left(\left\{2\left[\sqrt{1+i\omega\tau} + \frac{\lambda}{2}\left(\frac{1}{r_0}+\frac{1}{r_L}\right)\right] e^{(L/\lambda)\sqrt{1+i\omega\tau}} + \frac{\lambda^2}{r_0 r_L}\frac{\sinh\left[(L/\lambda)\sqrt{1+i\omega\tau}\right]}{\sqrt{1+i\omega\tau}}\right\}^{-1}\right). \tag{2.4}$$

Note that f is unitless and depends only on the scales L/λ, $\omega\tau$, and λ/r_i. The parameters r_i, with i either 0 for the left contact or L for the right, are

$$r_i = \frac{R_F + R_C^i}{R_{\mathrm{SQ}}} W, \tag{2.5}$$

where R_F is the resistance of the ferromagnet and R_C^i are the individual contact resistances, W is the graphene flake width, and

$$R_{\mathrm{SQ}} = W/\sigma^N, \tag{2.6}$$

is the graphene square (sheet) resistance given in terms of the semiconductor conductivity σ^N. The resistances R_F and R_C^i are the effective resistances of a unit cross sectional area. They are defined in equations (A.10) and (A.15). To obtain an expression in terms of the ohmic resistances, one must make the substitutions $R_F \to W_F W R_F$ and $R_C^i \to W_F W R_C^i$, where W_F is the contact width, i.e., $W_F W$ is

the contact area. We will use the same symbols for either resistance type when the meaning is clear. The polarizations p_1 and p_2, defined in equation (A.36), model the effective current injection. They depend on the resistances and the spin polarizations of the semiconductor and the individual contacts.

The expression $\Delta R_{\mathrm{NL}} = \left|R^{+}_{\mathrm{NL}} - R^{-}_{\mathrm{NL}}\right|$ measures the difference in signal between parallel and antiparallel field alignments. We combine $P^2 = |p_1 p_2|$,[1] and write

$$\Delta R_{\mathrm{NL}} = 2P^2 R_N |f|, \tag{2.7}$$

with

$$R_N = \frac{\lambda}{W}\frac{1}{\sigma_G}, \tag{2.8}$$

where $\sigma_G = \sigma^N L$ is the graphene conductance normally given in units of mS $= (\mathrm{m}\Omega)^{-1}$.

2.3 Fits

Data presented in figure 4 from [30] was fit to the model presented here. Fits were done using Python and matplotlib [3]. Links to the source code along with instructions on how to create similar fits and figures are available online.[2]

We assume similar contacts, $R_C = R^0_C = R^L_C$. The resistance of the ferromagnet Co is computed as $R_F = \rho_F \lambda_F / A_J$, where ρ_F is the Co resistivity, λ_F is the spin diffusion length of Co, and A_J is the junction area estimated at $A_J = Wd$, with d between 0.5 nm and 50 nm [30]. Hanle fits were done using a simple least squares

[1] Assuming the polarizations P^F_σ and P^L_Σ have the same sign bounds $P \leq 1$.

[2] An online portal with links to the code used to prepare this work is located at evansosenko.com/spin-lifetime.

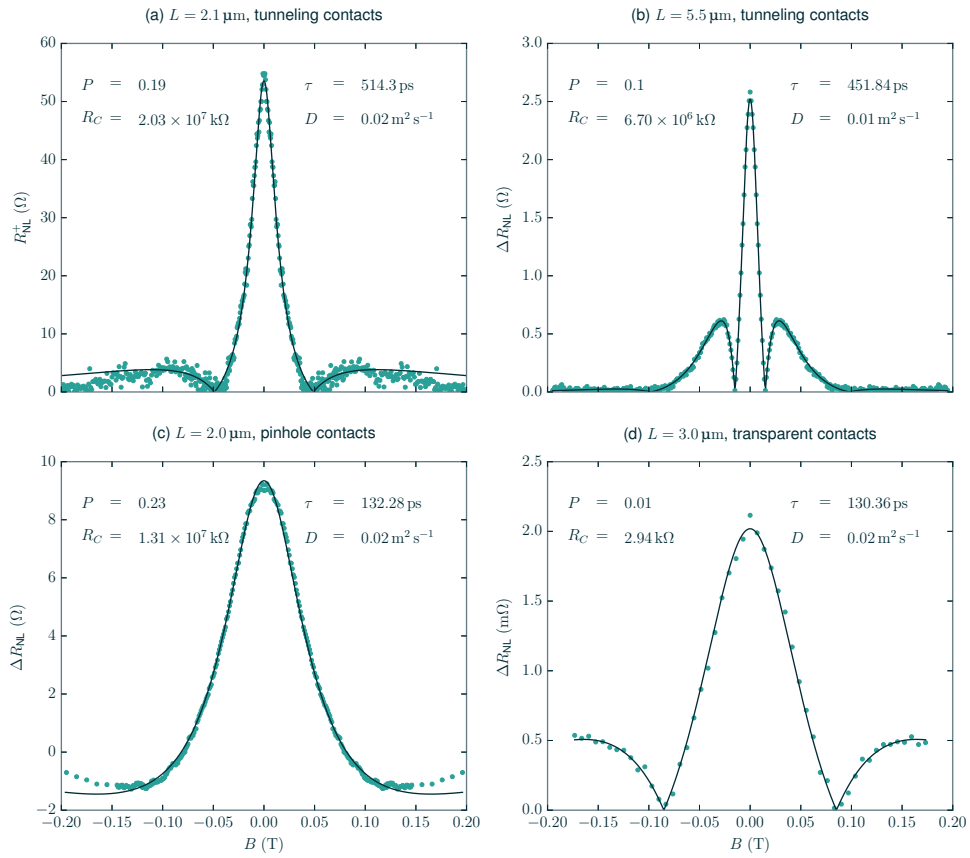

Figure 2.2: Data in figure 4 from [30] fit to equation (2.7) or equation (2.2) with the following values: $W = 2.2\,\mu\text{m}$, $W_F = 1.0\,\mu\text{m}$, $\sigma_G = 0.5\,\text{mS}$, $\rho_F = 60\,\Omega\,\text{nm}$, and $R_F = 3.27\,\Omega$ ($d = 0.5\,\text{nm}$ and $\lambda_F = 0.06\,\mu\text{m}$). The contact type (tunneling, pinhole, or transparent) and the contact separation L varies.

algorithm with nonnegative parameters τ, D, R_C, and P. The polarization P was constrained between zero and one.

Figure 2.2 shows fits of ΔR_{NL} given by equation (2.7) for devices with tunneling and transparent contacts, and R_{NL}^+ given by equation (2.2) for a device with pinhole contacts.[3] Fits (a), (b), and (c) with tunneling and pinhole contacts give large $R_C \sim$

[3]Parallel and antiparallel data for this device was only available at dissimilar field

$10^7\,\mathrm{k}\Omega$ and lifetimes equivalent to fitting with $R_C \to \infty$, while (d) with transparent contacts gives a reduced $R_C \sim 3\,\mathrm{k}\Omega$ and a lifetime increased by at most a factor of two (compare to 78 ps for $R_C \to \infty$). For tunneling contacts, the polarization P is 25 % to 60 % smaller than the lower bound given in [30], while for transparent contacts, P is reduced by an order of magnitude.

Note that we have used R_C as a fitting parameter. In most devices, this quantity can be experimentally determined, thus further constraining the fitting algorithm. As we will discuss further in the next section, a fact that becomes apparent from our analytic result is that the relevant scale is λ/r. Once r becomes larger than λ, all of the corrections to the $R_C \to \infty$ limit Hanle curves become very small. In other words, once $r \gg \lambda$, the fit is insensitive to the actual value of the contact resistance. The fact that we quote a resistance of order $10^7\,\mathrm{k}\Omega$ in fits (a), (b), and (c) in figure 2.2 results from the built-in accuracy we demand of the fitting algorithm. A good fit can be obtained for any r as long as it is larger than λ.

2.4 Regimes

In this section we discuss the various limits of the expression describing the Hanle precession curve. First, we show that the commonly used results for zero magnetic field and tunneling contacts are correctly reproduced. Next, we discuss regimes where appropriate scaling will give non-unique Hanle fits. In the following, we consider the case $r = r_0 = r_L$ of similar contacts.

In the limit of tunneling contacts, $R_C^0, R_C^L \gg R_F$. Putting $r_0, r_L \to \infty$ gives

values, thus ΔR_{NL} could not be fit.

$p_1 p_2 \to \left(P_\Sigma^L\right)^2$ and

$$f^\infty = \mathrm{Re}\,\frac{e^{-(L/\lambda)\sqrt{1+i\omega\tau}}}{2\sqrt{1+i\omega\tau}}, \tag{2.9}$$

which is of the same form as found in appendix B of [31] (we will denote this limit with the superscript ∞). Fitting with this expression was found to give results equivalent to fitting with the Hanle equation

$$R_{\mathrm{NL}}^{\pm} = \pm S_{\mathrm{NL}} \int_0^\infty \frac{e^{-t/\tau}}{\sqrt{4\pi D t}} \exp\left[-\frac{L^2}{4Dt}\right] \cos\omega t \; dt. \tag{2.10}$$

The agreement is expected as an explicit integration of equation (2.10) yields the same analytic expression with the identification $S_{\mathrm{NL}} = p_1 p_2 D/W\sigma_G$. In the additional limit of zero magnetic field,

$$\Delta R_{\mathrm{NL}} = \left(P_\Sigma^L\right)^2 R_N e^{-L/\lambda}, \tag{2.11}$$

which agrees with equation (6) in [28].

Let f_0 denote f at zero magnetic field,

$$f_0 = \left[2\left(1+\lambda/r\right)e^{L/\lambda} + \left(\lambda/r\right)^2 \sinh L/\lambda\right]^{-1}, \tag{2.12}$$

which agrees with equation (3) in [24].

To further explore the nature of the Hanle curves, we exploit the fact that it only depends on the dimensionless ratios λ/r, L/λ, and $\omega\tau$. The only other parameter of the conducting channel that enters the expression is the overall scale λ in R_N. The expression f contains three terms which are of zeroth, first, and second order in λ/r. Thus, as the contact resistance decreases, one goes from a device dominated by the first term to one dominated by the last. But precisely how this comes about depends on the value of $\omega\tau$.

For infinite contact resistance, it was pointed out that any rescaling of g, τ and D that leaves λ and $\omega\tau$ unchanged leads to the same Hanle precession curves [32]. Our result shows that the same is also true when the contact resistance is taken into account. In numerical simulations, interesting features were observed when $L/\lambda \ll 1$ and $r/\lambda \ll 1$ [33].

To compare across regimes, we first normalize the data to its value at zero magnetic field. In devices where $\lambda/r \gg 1$, the normalization factor is

$$f_0 = \frac{2e^{-L/\lambda}}{(\lambda/r)^2}. \tag{2.13}$$

In this regime, if D is not very different from the infinite contact resistance value, then the lifetime can be large, i.e., $\tau \gg 1\,\text{ns}$. As one tunes the magnetic field $\sqrt{\omega\tau} \gg 1$, for small values of the field, and for much of the curve, we can approximate $1+i\omega\tau \approx i\omega\tau$. An interesting consequence of this is that the zero of the Hanle precession curve becomes independent of the scattering time. Note that the product

$$\frac{L}{\lambda}\sqrt{\omega\tau} = L\sqrt{\frac{D}{\omega}}, \tag{2.14}$$

which appears in the exponential and oscillating factors below, is independent of the lifetime. As one further tunes the magnetic field, the Hanle curve is given by

$$f = \frac{\sqrt{\omega\tau}}{(\lambda/r)^2} e^{-(L/\lambda)\sqrt{\omega\tau/2}} \sin\left[\frac{L}{\lambda}\sqrt{\frac{\omega\tau}{2}} + \frac{\pi}{4}\right], \tag{2.15}$$

as long as $\lambda/r \gg \sqrt{\omega\tau} \gg 1$. In this limit, the nonlocal resistance scales as

$$\Delta R_{\text{NL}} \propto \frac{\lambda\sqrt{\omega\tau}}{(\lambda/r)^2} = r^2\sqrt{\frac{\omega}{D}}, \tag{2.16}$$

and the normalized nonlocal resistance as

$$f/f_0 \propto \sqrt{\omega\tau}. \tag{2.17}$$

On further increasing the field, $\sqrt{\omega\tau} \gg \lambda/r \gg 1$, we get

$$f = \frac{1}{2\sqrt{\omega\tau}} e^{-(L/\lambda)\sqrt{\omega\tau/2}} \cos\left[\frac{L}{\lambda}\sqrt{\frac{\omega\tau}{2}} + \frac{\pi}{4}\right]. \tag{2.18}$$

In this limit, the nonlocal resistance scales as

$$\Delta R_{\mathrm{NL}} \propto \frac{\lambda}{\sqrt{\omega\tau}} = \sqrt{\frac{D}{\omega}}, \tag{2.19}$$

and the normalized nonlocal resistance as

$$f/f_0 \propto \frac{(\lambda/r)^2}{\sqrt{\omega\tau}} = D\sqrt{\frac{\tau}{\omega r^4}}. \tag{2.20}$$

In the limits of equations (2.15) and (2.18), the zeros of the Hanle fit are independent of the lifetime and are determined by D though the condition

$$L\sqrt{\frac{D}{2\omega}} + \frac{\pi}{4} = \frac{n\pi}{2}, \tag{2.21}$$

where $n = 0$ for equation (2.15) and $n = 1$ for equation (2.18).

Note that fitting is insensitive to τ in the limit of equation (2.16) or equation (2.19). As an example of this, figure 2.3 shows nearly identical fits with lifetimes that differ by four orders of magnitude. These fits were obtained by choosing large starting values for τ. For figure 2.2 (d) and figure 2.3, $\chi^2 \sim 7 \times 10^{-8}$, but the χ^2 for figure 2.2 (d) is 2 % less than the χ^2 for figure 2.3. In figure 2.2 (d), $\lambda/r \gg \sqrt{\omega\tau}$ and $\omega\tau \sim 1$ for most of the curve, so the approximation $1 + i\omega\tau \approx i\omega\tau$ does not hold. However, figure 2.3 is in the limit of equation (2.16) for all points (save the origin). Thus, in limit of small r, the fitted value of τ is unreliable unless one carefully controls the fitting procedure.

The evolution of the expression for the Hanle curve is an interesting insight into the behavior of the device. Fitting data on devices with small contact resistances

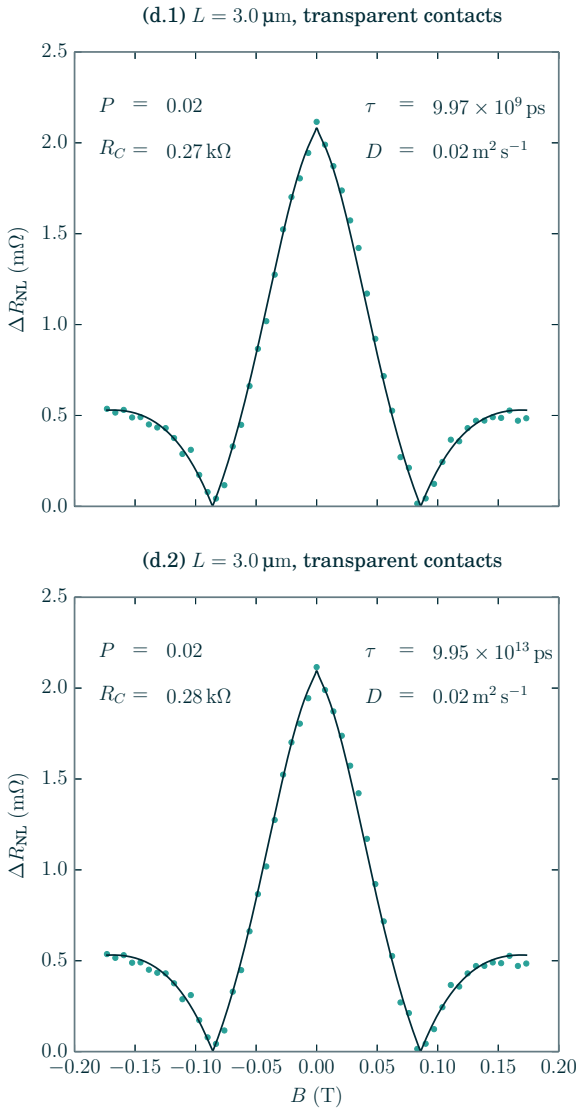

Figure 2.3: Data in figure 4 (d) from [30] fit to equation (2.2) with the same values as in figure 2.2 (d). Fits with lifetimes that differ by four orders of magnitude were obtained by using different starting values for τ. These fits are otherwise similar with the exception of the lifetime, demonstrating the τ-independent scaling in equation (2.16). The χ^2 for figure 2.2 (d) is 2 % less than the χ^2 for figure 2.3.

with the functional form applicable to infinite contact resistance yields unreliable parameters. In particular, they were numerically shown to severely underestimate the spin lifetime [33].

Further analytic progress can be made if one assumes that lifetimes as estimated with infinite contact resistance are long enough that the approximation of $\sqrt{\omega\tau} \gg \lambda/r \gg 1$ is still valid for much of the data being analyzed. For this case, at infinite contact resistance, the normalized nonlocal resistance is given by

$$\frac{f^{\infty}}{f_0^{\infty}} = \frac{1}{\sqrt{\omega\tau}} e^{-(L/\lambda)\sqrt{\omega\tau/2}} \cos\left[\frac{L}{\lambda}\sqrt{\frac{\omega\tau}{2}} + \frac{\pi}{4}\right]. \tag{2.22}$$

Provided D remains constant, this will yield the same curve with finite contact resistance if

$$\frac{1}{\tau^{\infty}} = D^2 \frac{\tau}{r^4}. \tag{2.23}$$

In other words, if we fix τ and ask what happens to the fitted value assuming infinite contact resistance as a function of decreasing r, equation (2.23) shows that it will decrease as well. For D fixed, $\tau^{\infty} \propto r^4$. While the general trend is consistent with [33], the quantitative agreement is limited by the approximations made for analytic convenience.

Chapter 3

TMD Superconductivity

3.1 Introduction

The interplay of spin-orbit interaction and electron-electron interaction is a fertile area of research where new phases of matter and novel phenomena have been theoretically conjectured and experimentally realized [34–40]. Single-layer transition metal group-VI dichalcogenides (TMDs), MX_2 ($M = Mo, W$ and $X = S, Se, Te$), are direct band gap semiconductors that have all the necessary ingredients to explore these phenomena [41–51]. While sharing the hexagonal crystal structure of graphene, they differ in three important aspects: (1) inversion symmetry is broken, resulting in a gap as opposed to Dirac nodes; (2) spin is coupled to momenta, yielding a large splitting of the valence bands; and (3) the bands near the chemical potential predominantly have the transition metal d-orbital character [52–57].

The nontrivial Berry curvature associated with the bands near the valleys is a consequence of strong spin-orbit coupling enabled by inversion symmetry breaking and heavy elements such as Mo and W. The Berry curvature engenders an effective

intrinsic angular momentum associated with the Bloch wave functions. Remarkably, spin-preserving optical transitions between valence and conduction bands are possible, even though the atomic orbitals involved all have a d-character. Furthermore, the valley-dependent sign of the Berry curvature leads to selective photoexcitation: right circular polarization couples to one valley, and left circular polarization to the other. Consequently, this enables a number of valleytronic and spintronic applications that have attracted a lot of attention over the last few years [58–60].

We are primarily interested in exploiting the band structure and valley-contrasting probe afforded by the nontrivial topology in order to study and manipulate correlated phenomena in these systems. In particular, we focus on hole-doped systems, where an experimentally accessible window in energy is characterized by two disconnected pieces of spin non-degenerate Fermi surfaces. One can preferentially excite electrons from either Fermi surface. Since the spins are locked to their valley index, these excitations have specific s_z (where the z-axis is perpendicular to the two-dimensional crystal). We focus on the possible superconducting states and their properties.

Spin-valley locking and its consequence for superconductivity, dubbed Ising superconductivity, has been previously studied for heavily doped p-type and n-type TMDs [61–65], where Fermi surfaces of each spin are present in each valley. Our focus is the regime of maximal loss of spin degeneracy where the effects are most striking [66]. The two valleys in the energy landscape generically allow two classes of superconducting phases: intervalley pairing with zero center of mass momentum, and intravalley pairing with finite Cooper pair center of mass. Since center-of-symmetry is broken and spin degeneracy is lost, classifications of superconducting states by parity, i.e., singlet vs. triplet, is no longer possible. In this chapter, we study both extrinsic and intrinsic superconductivity by projecting the interactions and pairing potential to the

topmost valence band. We identify the possible phases, and analyze the nature of the optoelectronic coupling. Our main conclusions are as follows:

(1) For both proximity to an s-wave superconductor, and due to local attractive density-density interactions, the leading instability is due to an intervalley paired state, where the Cooper pair is an equal mixture of a spin singlet and the $m = 0$ spin triplet [67].

(2) While the valley selectivity of the optical transition is suppressed, it remains finite. Consequently, the two quasiparticles generated by pair-breaking circularly polarized light are correlated such that one is in the valence band of one valley and the conduction band of the other. The valley and bands are determined by the polarity of incident light.

(3) The quasiparticles generated in (2) both have the same charge and Berry curvature. Thus an anomalous Hall effect is anticipated as the two travel in the same direction transverse to an applied electric field.

3.2 Model

The TMD system is described by the effective tight-biding, low-energy, two-valley Hamiltonian [59],

$$H_{\tau}^{0}\left(\mathbf{k}\right)=at\left(\tau k_{x}\sigma_{x}+k_{y}\sigma_{y}\right)\otimes I_{2}+\frac{\Delta}{2}\sigma_{z}\otimes I_{2}-\lambda\tau\left(\sigma_{z}-1\right)\otimes S_{z}. \tag{3.1}$$

The (periodic) Bloch orbital states (see appendix B) are

$$\left|v_{\tau s}^{\nu}\left(\mathbf{k}\right)\right\rangle=\frac{T_{\mathbf{k}+\tau\mathbf{K}}}{\sqrt{N}}\sum_{n=1}^{N}e^{i\left(\mathbf{k}+\tau\mathbf{K}\right)\cdot\mathbf{R}_{n}^{0}}T\left(\mathbf{R}_{n}^{0}\right)\left|\varphi_{\tau s}^{\nu}\right\rangle, \tag{3.2}$$

where N is the number of M-type atoms in the system,

$$|\varphi^{+}_{\tau s}\rangle = |d_{z^2}\rangle \otimes |s\rangle\,, \tag{3.3a}$$

$$|\varphi^{-}_{\tau s}\rangle = \frac{1}{\sqrt{2}}\left(\left|d_{x^2-y^2}\right\rangle + i\tau\left|d_{xy}\right\rangle\right) \otimes |s\rangle\,, \tag{3.3b}$$

and $\left|d_{xy}\right\rangle$ and $\left|d_{x^2-y^2}\right\rangle$ refer to the angular momentum orbitals in the symmetry group $E\left(d_{xy}, d_{x^2-y^2}\right)$. The operators σ_i are Pauli operators acting on the two Bloch orbital states (indexed by $\nu = \pm$) such that $\sigma_z\left|v^{\pm}_{\tau s}(\mathbf{k})\right\rangle = \pm\left|v^{\pm}_{\tau s}(\mathbf{k})\right\rangle$. The valley index $\tau = \pm$, corresponding to the $\pm\mathbf{K}$ points, and the spin index $s = \pm$ (or $s = \uparrow\downarrow$), corresponding to the z-component of the spin through $s_z = s/2$, are good quantum numbers.[1] The momentum $\mathbf{k}$ is measured from the valley center, i.e., for a given valley, the total momentum relative to the center of the Brillouin zone is $\mathbf{k} + \tau\mathbf{K}$. The energy gap is Δ, the spin splitting in the valence band is 2λ, the lattice constant is a, and t is the effective hopping integral. Equation (3.1) can be written in matrix form in the Bloch orbital basis,

$$\left[H^{0}_{\tau s}(\mathbf{k})\right] = \begin{bmatrix} \dfrac{\Delta}{2} & at\left(\tau k_x - ik_y\right) \\ at\left(\tau k_x + ik_y\right) & \lambda\tau s - \dfrac{\Delta}{2} \end{bmatrix}. \tag{3.4}$$

The energy spectrum,

$$E^{n}_{\tau s}(k) = \frac{1}{2}\left(\lambda\tau s + n\sqrt{(2atk)^2 + (\Delta - \lambda\tau s)^2}\right), \tag{3.5}$$

with $k = |\mathbf{k}|$ and $n = 1$ ($n = -1$) indexing the conduction (valence) band is shown in figure 3.1. For a fixed band, we have the inverse relation,

$$\left(\frac{atk}{\Delta/2}\right)^2 = \left(\frac{2E}{\Delta}\right)^2 + 2\tau s\left(\frac{\lambda}{\Delta}\right)\left(1 - \frac{2E}{\Delta}\right) - 1, \tag{3.6}$$

[1] Only in this chapter do we use s to denote spin. In the appendices, we adopt the more traditional symbol σ.

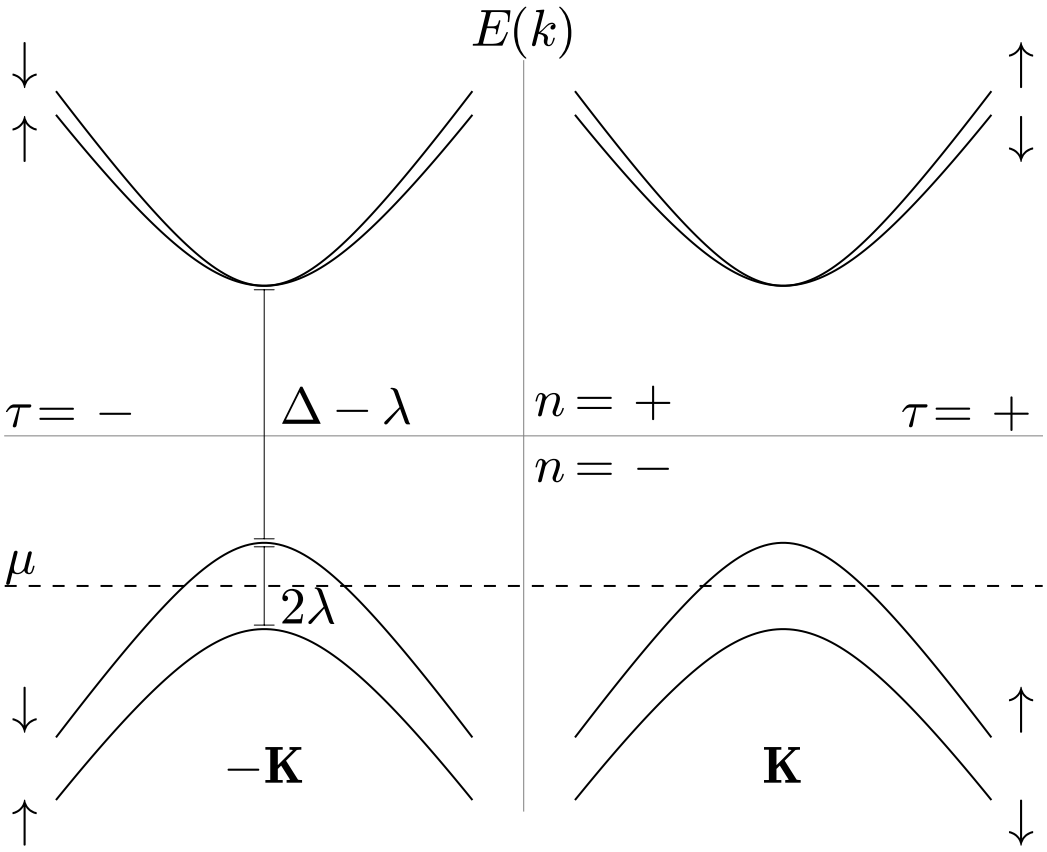

Figure 3.1: Energy bands for WSe_2 as given by equation (3.5) with $at = 3.939\,\text{eV}\,\text{Å}^{-1}$, $\Delta = 1.60\,\text{eV}$, and $\lambda = 0.23\,\text{eV}$. Each valley is centered at $\pm\mathbf{K}$ relative to the center of the Brillouin zone. The energy for a given band depends only on the distance k measured from the valley center.

where $E > \Delta/2$ for $n = 1$ and $E < -(\Delta/2 - \lambda\tau s)$ for $n = -1$. Note the relations

$$\theta^n_{-\downarrow}(k) + \theta^n_{+\uparrow}(k) = 2\pi, \tag{3.7a}$$

$$\theta^+_{\tau s}(k) - \theta^-_{\tau s}(k) = -\tau\pi, \tag{3.7b}$$

$$\phi_{-\mathbf{k}} - \phi_{\mathbf{k}} = \pi. \tag{3.7c}$$

We focus on doped systems such that the chemical potential μ lies in the upper valence bands. Within each band, the Bloch basis eigenstates are written in terms of

the orbital states as elements on the Block sphere,

$$\left|u_{\tau s}^{n}\left(k,\phi\right)\right\rangle =\cos\frac{\theta_{\tau s}^{n}\left(k\right)}{2}\left|v_{\tau s}^{+}\left(k,\phi\right)\right\rangle +e^{-i\tau\phi}\sin\frac{\theta_{\tau s}^{n}\left(k\right)}{2}\left|v_{\tau s}^{-}\left(k,\phi\right)\right\rangle ,\tag{3.8}$$

where $k_x + i\tau k_y = ke^{i\tau\phi}$ and

$$\tan\frac{\theta_{\tau s}^{n}\left(k\right)}{2}=\frac{at\tau k}{\frac{\Delta}{2}-E_{\tau s}^{-n}\left(k\right)}=\frac{at\tau k}{E_{\tau s}^{n}\left(k\right)-E_{\tau s}^{-}\left(0\right)}.\tag{3.9}$$

The polar angle on the Bloch sphere of the conduction and valence bands are related by $\theta_{\tau s}^{-}\left(k\right)-\theta_{\tau s}^{+}\left(k\right)=\tau\pi$. The mapping of the energy band to the Bloch sphere, parametrized by (θ,ϕ), encodes the topological character: as one moves from the node out to infinity, the states sweep either the northern or southern hemisphere with a chirality determined by the Berry curvature.

3.3 Superconductivity

We consider two approaches to realizing a superconducting state. First, we assume a proximity induced state obtained by layering a TMD on an s-wave superconductor. Second, we study an intrinsic correlated phase arising from density-density interactions.

We use $d_{\tau s}^{\nu}\left(\mathbf{k}\right)$ as the annihilation operator for tight-binding d-orbital states,[2] and $c_{\tau s}^{n}\left(\mathbf{k}\right)$ for the eigenstates of the non-interacting Hamiltonian, $\lambda_{\mathbf{k}}$ for the energy dispersion for Bogoliubov quasiparticles, and $\Delta_{\mathbf{k}}$ for the superconducting gap function. A review of interaction theory may be found in appendix C, and additional computational detail for the intrinsic case is given in appendix D.

[2]In this chapter we use d for these operators, however in the appendices, we use a to match the tight-binding notation.

Induced State

A proximity s-wave superconductor will inject Cooper pairs according to

$$H^V = \sum_{\mathbf{k},\nu,\tau} \bar{B}_\nu d^\nu_{-\tau\downarrow}(-\mathbf{k})\, d^\nu_{\tau\uparrow}(\mathbf{k}) + \frac{\varepsilon}{2} + \text{h.c.} \tag{3.10}$$

The coupling constants B_ν and the overall constant ε depend on the material interface.[3] Using the abbreviated notation $c_{\mathbf{k}\alpha} = c^-_{\tau s}(\mathbf{k})$, with $\alpha = \uparrow\downarrow$ for $\tau = s = \pm$, projecting onto the upper valence bands yields,

$$\begin{aligned} &P^{n=-}_{\tau=s}\left(H^0 + H^V - \mu N\right) \\ &\qquad = \sum_{\mathbf{k},\alpha} \xi_{\mathbf{k}} c^\dagger_{\mathbf{k}\alpha} c_{\mathbf{k}\alpha} - \sum_{\mathbf{k}} \left(\bar{\Delta}_{\mathbf{k}} c_{-\mathbf{k}\downarrow} c_{\mathbf{k}\uparrow} + \Delta_{\mathbf{k}} c^\dagger_{\mathbf{k}\uparrow} c^\dagger_{-\mathbf{k}\downarrow}\right) + \varepsilon, \end{aligned} \tag{3.11}$$

where $\xi_{\mathbf{k}} = E^-_{+\uparrow}(|\mathbf{k}|) - \mu$ and the effective BCS gap function is

$$\Delta_{\mathbf{k}} = \frac{1}{2}\left(B_+ + B_-\right) + \frac{1}{2}\left(B_+ - B_-\right)\cos\theta_{\mathbf{k}}, \tag{3.12}$$

with $\theta_{\mathbf{k}} = \theta^-_{+\uparrow}(|\mathbf{k}|)$.[4] This form is identical to the standard BCS Hamiltonian with an effective spin index α. However, the spin state of the Cooper pair is an equal superposition of the singlet and the $m = 0$ component of spin triplet. The corresponding quasiparticle eigenstates are $\gamma_{\mathbf{k}\alpha} = \alpha\cos\beta_{\mathbf{k}} c_{\mathbf{k}\alpha} + \sin\beta_{\mathbf{k}} c^\dagger_{-\mathbf{k},-\alpha}$, [5] with energies $\lambda_{\mathbf{k}} = \pm\sqrt{\xi^2_{\mathbf{k}} + \Delta^2_{\mathbf{k}}}$, where $\cos 2\beta_{\mathbf{k}} = \xi_{\mathbf{k}}/\lambda_{\mathbf{k}}$. Note that if $B_+ = B_-$, then $\Delta_{\mathbf{k}}$ is a constant and independent of $\mathbf{k}$. Even when B_+ and B_- are different, the constant term dominates. Before exploring the nature of this state, we analyze the case of intrinsic superconductivity, and show that the same state is energetically preferred.

[3] Note that all sums over $\mathbf{k}$ are restricted to $|\mathbf{k}|$ less than some cutoff that restricts the momentum to a single valley.

[4] We may take $\Delta_{\mathbf{k}}$ to be real. Otherwise, if $\Delta_{\mathbf{k}} = |\Delta_{\mathbf{k}}| e^{i\arg\Delta_{\mathbf{k}}}$, then make the unitary transformation $c_{\mathbf{k}\alpha} \to e^{i\arg\Delta_{\mathbf{k}}/2} c_{\mathbf{k}\alpha}$.

[5] In this chapter we use γ for these operators, however in the appendices, we use b to avoid other notational conflicts.

Intrinsic Phase

For a local attractive density-density interaction (e.g. one mediated by phonons), the potential is $V \backsimeq \frac{1}{2}\sum_{\mathbf{R},\mathbf{R}'} v_{\mathbf{R}\mathbf{R}'} :n_{\mathbf{R}} n_{\mathbf{R}'}:$, with $v_{\mathbf{R}\mathbf{R}'} = v_0 \delta_{\mathbf{R}\mathbf{R}'}$ and $n_{\mathbf{R}}$ the total Wannier electron density at lattice vector $\mathbf{R}$. Projecting onto states near the chemical potential gives

$$P_{\tau=s}^{n=-}\left(H^V\right) = \sum_{\mathbf{k},\mathbf{k}'} v\left(\mathbf{k}'-\mathbf{k}\right)\Big(2|A_{\mathbf{k}\mathbf{k}'}|^2 c^\dagger_{\mathbf{k}'\uparrow} c^\dagger_{-\mathbf{k}'\downarrow} c_{-\mathbf{k}\downarrow} c_{\mathbf{k}\uparrow} + A^2_{\mathbf{k}\mathbf{k}'} c^\dagger_{\mathbf{k}'\uparrow} c^\dagger_{-\mathbf{k}'\uparrow} c_{-\mathbf{k}\uparrow} c_{\mathbf{k}\uparrow} + A^2_{\mathbf{k}'\mathbf{k}} c^\dagger_{\mathbf{k}'\downarrow} c^\dagger_{-\mathbf{k}'\downarrow} c_{-\mathbf{k}\downarrow} c_{\mathbf{k}\downarrow}\Big), \quad (3.13)$$

where

$$A_{\mathbf{k}\mathbf{k}'} = e^{i(\phi_{\mathbf{k}'}-\phi_{\mathbf{k}})} \sin\frac{\theta_{\mathbf{k}'}}{2}\sin\frac{\theta_{\mathbf{k}}}{2} + \cos\frac{\theta_{\mathbf{k}'}}{2}\cos\frac{\theta_{\mathbf{k}}}{2}. \quad (3.14)$$

The first term in equation (3.13) leads to intervalley pairing, and last two lead to intravalley pairing. We analyze the possible states within mean field theory. The BCS order parameter is

$$\chi = v_0 \sum_{\mathbf{k}} \bar{g}_{\mathbf{k}} \left\langle c_{-\mathbf{k}\alpha'} c_{\mathbf{k}\alpha}\right\rangle, \quad (3.15)$$

where the form of $g_{\mathbf{k}}$ depends on the particular pairing channel. The resulting Hamiltonian has the same form as the BCS Hamiltonian in equation (3.11) but with an effective $\Delta_{\mathbf{k}} = g_{\mathbf{k}} \cdot \chi$. The intravalley pairing has three symmetry channels, with the couplings given by $2g_{\mathbf{k}} = 1+\cos\theta_{\mathbf{k}}$, $\sqrt{2}e^{-i\phi_{\mathbf{k}}} g_{\mathbf{k}} = \sin\theta_{\mathbf{k}}$, and $2e^{-2i\phi_{\mathbf{k}}} g_{\mathbf{k}} = 1-\cos\theta_{\mathbf{k}}$. For these channels, since $\left\langle c_{-\mathbf{k}\alpha} c_{\mathbf{k}\alpha}\right\rangle = -\left\langle c_{\mathbf{k}\alpha} c_{-\mathbf{k}\alpha}\right\rangle$, relabeling $\mathbf{k} \to -\mathbf{k}$ in the sum gives $\chi = 0$.[6] The intervalley pairing also has three symmetry channels: $g_{\mathbf{k}} = \sqrt{2}$, $g_{\mathbf{k}} = \sqrt{2}\cos\theta_{\mathbf{k}}$, and $g_{\mathbf{k}} = \sqrt{2}\sin\theta_{\mathbf{k}}\hat{\mathbf{k}}$. Of the three, the constant valued channel is

[6] For odd parity interactions, where $v\left(-\mathbf{k}\right) = -v\left(\mathbf{k}\right)$, the intravalley pairing is not excluded by symmetry. Specifically, repeating the calculation with this assumption, the intervalley terms fully cancel, and one obtains equation (3.13) without the intervalley term on the first line.

dominant.[7] This is to be expected, as the local density-density interaction leads to the largest pairing for electrons of opposite spins. Since the intravalley processes have the same spin, they are disfavored as compared to the intervalley pairing.

The key features of the intrinsic superconducting state are identical to the proximally induced case when density-density interactions dominate. We restrict further analysis to that case, and turn to the question of optically induced pair-breaking phenomena.

3.4 Optoelectronic coupling

The non-interacting system displays valley selective optical excitations. Light of a particular polarization only couples to one valley. Since the superconducting state is a coherent condensate admixing the two valleys, we address whether pair-breaking displays similar valley selectivity. In particular, we explore whether or not the two quasiparticles generated by circularly polarized light, with total energy larger than $\Delta + \Delta_{\mathbf{k}}$, occupy opposite valleys, with one in the conduction band and the other in the valence band.

The optical excitations arise from the Berry curvature, which acts as an effective angular momentum. The electromagnetic potential $\mathbf{A}$, with polarization vector $\boldsymbol{\epsilon}$, is introduced using minimal coupling, $H^{\nu\nu'}_{\tau s}(\mathbf{k}) \to H^{\nu\nu'}_{\tau s}(\mathbf{k} + e\mathbf{A})$, where, in the dipole approximation, $\mathbf{A} = 2\,\mathrm{Re}\,\boldsymbol{\epsilon} A_0 e^{-i\omega t}$. This yields a perturbed Hamiltonian $H \to H + H^A$, where $H^A = H' e^{-i\omega t} + H'^{\dagger} e^{i\omega t}$, with

$$H' = \sum_{\mathbf{k},\tau,s} H'_{\tau} d^{-}_{\tau s}{}^{\dagger}(\mathbf{k})\, d^{+}_{\tau s}(\mathbf{k}) - \sum_{\mathbf{k},\tau,s} H'_{-\tau} d^{+}_{\tau s}{}^{\dagger}(\mathbf{k})\, d^{-}_{\tau s}(\mathbf{k}), \tag{3.16}$$

[7] For example, using the values for WSe_2, $\sin^2\theta_{\mathbf{k}} = 0.44$ and $\cos^2\theta_{\mathbf{k}} = 0.56$ at the chemical potential.

and $H'_\tau = ateA_0 \left(\tau\hat{\mathbf{x}} + i\hat{\mathbf{y}}\right) \cdot \boldsymbol{\epsilon}$. The transition rate is proportional to the modulus-squared of the optical matrix elements, $\mathbf{P}_{\tau s}^{nn'}(\mathbf{k})$, defined by

$$H^A = \sum_{\substack{\mathbf{k},\tau,s \\ n,n'}} \frac{eA_0}{m_0} \boldsymbol{\epsilon} \cdot \mathbf{P}_{\tau s}^{nn'}(\mathbf{k})\, c_{\tau s}^{n\,\dagger}(\mathbf{k})\, c_{\tau s}^{n'}(\mathbf{k}). \tag{3.17}$$

For circularly polarized light, in the absence of superconductivity, $\boldsymbol{\epsilon}_\pm = \left(\hat{\mathbf{x}} \pm i\hat{\mathbf{y}}\right)/\sqrt{2}$ and

$$\boldsymbol{\epsilon}_\pm \cdot \mathbf{P}_{\tau s}^{+-}(\mathbf{k}) = \mp\tau\sqrt{2}atm_0 e^{\pm i\phi} \sin^2 \frac{\theta_{\tau s}^{\mp\tau}(k)}{2}. \tag{3.18}$$

See appendix E for a full derivation.

The transition rate matrix elements for optical excitations from the BCS ground state are given by equation (3.18) multiplied by a coherence factor $\sin\beta_{\mathbf{k}}$. Since $\theta_{\tau s}^{-}(k) - \theta_{\tau s}^{+}(k) = \tau\pi$, switching either the valley or polarization transforms $\sin \to \cos$ in equation (3.18), giving matrix elements $\left|P_\pm\right| = \left|\boldsymbol{\epsilon}_\pm \cdot \mathbf{P}_{++}^{+-}(\mathbf{k}) \sin\beta_{\mathbf{k}}\right|$ corresponding to matching (P_+) or mismatching (P_-) polarization-valley indexes. For a given valley, a chosen polarization of light couples more strongly than the other, as is evident comparing $|P_+|^2$ to $|P_-|^2$ and shown in figure 3.2. For incident light with energy $\Delta + |\lambda_{\mathbf{k}}|$, right circularly polarized light (+) has a higher probability of promoting a quasiparticle to the right conduction band, as reflected in the larger matrix element $|P_+|^2 \gg |P_-|^2$. As depicted in figure 3.3, the partner of the Cooper pair is in the valence band in the opposite valley. The other valley has the opposite dependence on polarization.

This key new result opens the door for valley control of excitations from a coherent ground state. For example, the two quasiparticles have the same charge and Berry curvature (see below). In the presence of an electric filed, they both acquire the same

transverse anomalous velocity. Thus, in contrast to the response in the normal state, an anomalous Hall effect is anticipated with no accompanying spin current.

3.5 Berry curvature

The Berry curvature in the non-interacting crystal for left and right circularly polarized ($\boldsymbol{\epsilon}_{\pm}$) optical excitations for a given $\mathbf{k}$ is $\pm 2\Omega^{+}_{+\uparrow}(k)$, where

$$\Omega^{n}_{\tau s}(k) = \hat{\mathbf{z}} \cdot \boldsymbol{\Omega}^{n}_{\tau s}(\mathbf{k}), \tag{3.19a}$$

$$= -n\tau \left[\frac{1}{2k}\frac{\partial}{\partial k}\theta^{n}_{\tau s}(k)\right] \sin\theta^{n}_{\tau s}(k), \tag{3.19b}$$

$$= -n\tau \frac{2(at)^2(\Delta - \lambda\tau s)}{\left[(2atk)^2 + (\Delta - \lambda\tau s)^2\right]^{3/2}}. \tag{3.19c}$$

The BCS ground state is[8]

$$|\Omega\rangle = \prod_{\mathbf{k}} \csc\beta_{\mathbf{k}} \gamma_{\mathbf{k}\uparrow}\gamma_{-\mathbf{k}\downarrow}|0\rangle, \tag{3.20a}$$

$$= \prod_{\mathbf{k}} \left(\cos\beta_{\mathbf{k}} - \sin\beta_{\mathbf{k}} c^{\dagger}_{\mathbf{k}\uparrow} c^{\dagger}_{-\mathbf{k}\downarrow}\right)|0\rangle. \tag{3.20b}$$

This superconducting state is built up from the quasiparticle eigenstates, $|\mathbf{k}\rangle = \csc\beta_{\mathbf{k}}\gamma_{\mathbf{k}\uparrow}\gamma_{-\mathbf{k}\downarrow}|0\rangle$, of the $\mathbf{k}$-dependent Hamiltonian $\lambda_{\mathbf{k}}\left(\gamma^{\dagger}_{\mathbf{k}\uparrow}\gamma_{\mathbf{k}\uparrow} + \gamma^{\dagger}_{-\mathbf{k}\downarrow}\gamma_{-\mathbf{k}\downarrow}\right)$. The z-component of the Berry curvature of the correlated state is zero,

$$\hat{\mathbf{z}} \cdot i\nabla_{\mathbf{k}} \times \langle \mathbf{k} | \nabla_{\mathbf{k}} | \mathbf{k}\rangle = \Omega^{-}_{+\uparrow}(k) + \Omega^{-}_{-\downarrow}(-k) = 0. \tag{3.21}$$

A single optically excited state in the left valley for a given $\mathbf{k}$ is ${c^{+}_{+\uparrow}}^{\dagger}(\mathbf{k})\, c^{-}_{+\uparrow}|\mathbf{k}\rangle$, which has a Berry curvature $+2\sin^6\beta_{\mathbf{k}}\Omega^{+}_{+\uparrow}(k)$. The corresponding excitation in the right valley has a Berry curvature of the same magnitude but opposite sign. See section D.4 for explicit computation of the above results.

[8]Note that the full ground state also contains the two lower filled bands, but those contribute zero net Berry curvature and may be ignored in this section and the next.

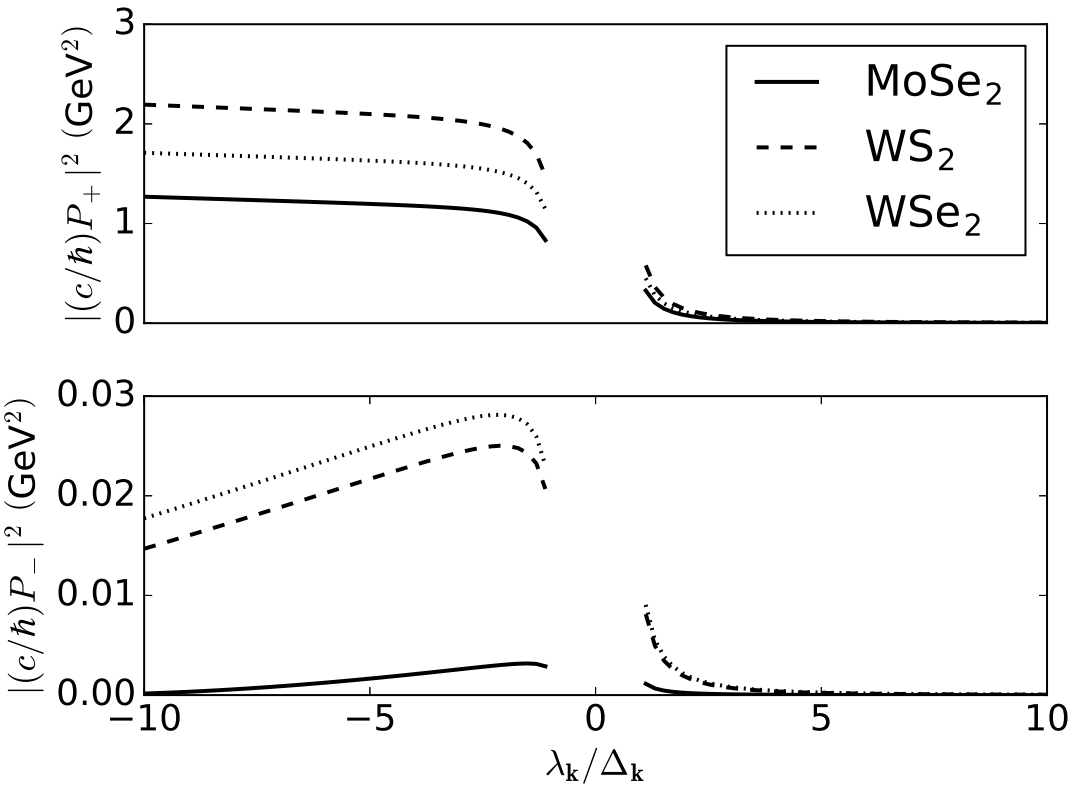

Figure 3.2: Optical transition rate matrix elements $\left|P_{\pm}\right|^2$ in the superconducting phase as a function of the ratio of the quasiparticle energy $\lambda_{\mathbf{k}}$ to the superconducting gap $\Delta_{\mathbf{k}}$. Material parameters for $MoSe_2$, WS_2, and WSe_2 are given in [59] and a gap of $\Delta_{\mathbf{k}} = 7.5\,\text{meV}$ is chosen for illustrative purposes. The order-of-magnitude contrast between $|P_+|^2$ and $|P_-|^2$ causes the optical-valley selectivity.

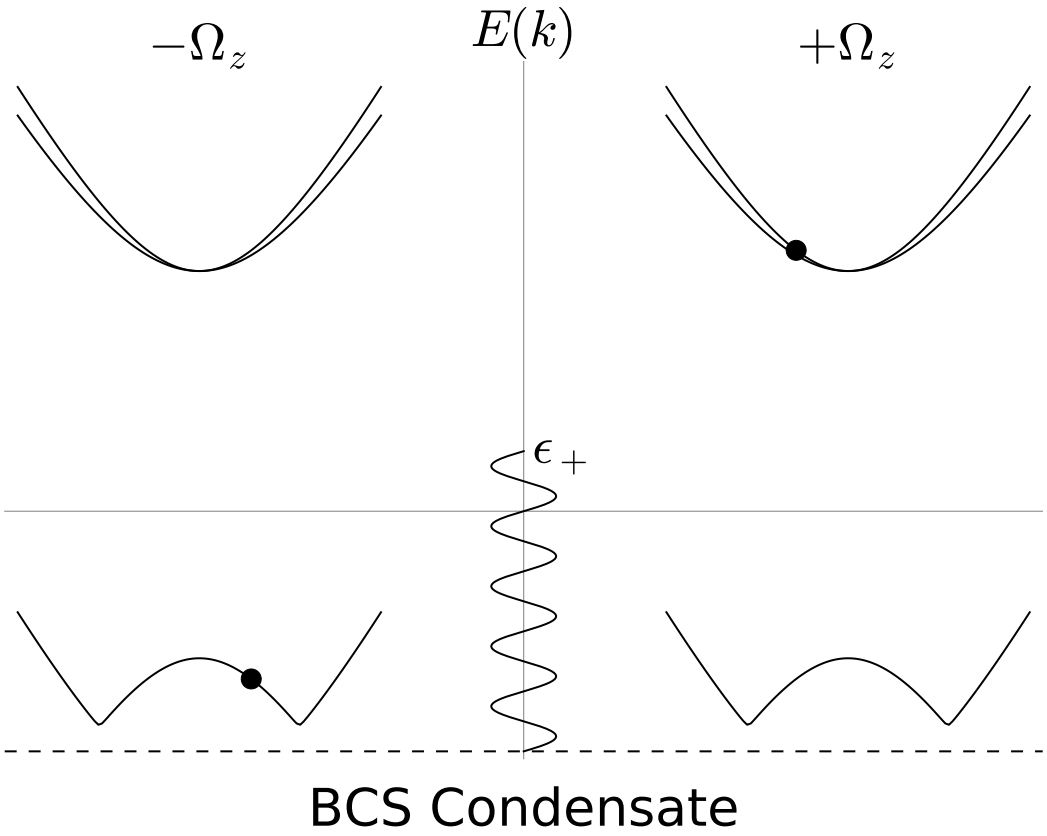

Figure 3.3: Pair-breaking by right circularly polarized light leads to an electron in the conduction band of the right valley and a partner in the valence band of the left valley. The valleys interchange for left circularly polarized light.

Chapter 4

Conclusion

In chapter 2 we have analyzed the effect of contact resistance on spin lifetimes determined via the Hanle spin precession technique in nonlocal spin valves. The general expression for the precession curves given in equation (2.4) is the main new result. While aspects of the discussed phenomena have been addressed numerically before, an analytic solution is obtained here which allows for detailed characterization of the device. In particular, general features of scaling as well as various limits and regimes can be analyzed. In addition, the solution allows for fitting data using standard curve fitting algorithms.

In chapter 3, we have reported on the nature of the superconducting state of hole-doped TMDs. Remarkably, the correlated state inherits the valley contrasting phenomena of the non-interacting state. While the magnitude is smaller, pair-breaking produces quasiparticles that have the same Berry curvature, and hence the same anomalous velocity. Thus one predicts an anomalous Hall response unlike the valley Hall response observed in $MoSe_2$. While systematic synthesis and characterization of hole-doped systems is still in its early stages, the fact that other two-dimensional com-

pounds and their bulk counterparts are known to be superconducting [68] provides impetus to explore this novel phenomena.

Appendix A

Nonlocal Resistance Derivation

In this appendix we derive an expression for the nonlocal resistance for finite contact resistance. We first present the key definitions and critical boundary conditions. We then derive the relation between the nonlocal resistance and the spin chemical potential at the far contact, $\mu_s^N(L)$. Finally, we solve the diffusion equation inside the semiconductor to find $\mu_s^N(L)$.

A.1 Definitions

Many of the definitions and results in this section are taken from [69]. The chemical potential and spin chemical potential are defined in terms of the spin-up and spin-down chemical potentials,

$$\mu = \frac{1}{2}\left(\mu_\uparrow + \mu_\downarrow\right), \tag{A.1a}$$

$$\mu_s = \frac{1}{2}\left(\mu_\uparrow - \mu_\downarrow\right). \tag{A.1b}$$

The material conductances and polarization are defined in terms of the spin-up and spin-down conductances,

$$\sigma = \sigma_\uparrow + \sigma_\downarrow, \tag{A.2a}$$

$$\sigma_s = \sigma_\uparrow - \sigma_\downarrow, \tag{A.2b}$$

$$P_\sigma = \frac{\sigma_s}{\sigma}. \tag{A.2c}$$

The gradient of the chemical potentials drives a current and spin current,

$$J_{\uparrow\downarrow} = \sigma_{\uparrow\downarrow} \nabla \mu_{\uparrow\downarrow}, \tag{A.3a}$$

$$J = J_\uparrow + J_\downarrow = \sigma \nabla \mu + \sigma_s \nabla \mu_s, \tag{A.3b}$$

$$J_s = J_\uparrow - J_\downarrow = \sigma_s \nabla \mu + \sigma \nabla \mu_s. \tag{A.3c}$$

To indicate the material, any of the above can have a superscript N (normal semiconductor) or F (ferromagnet).

The contact conductances and polarization are defined in terms of the spin-up and spin-down contact conductances,

$$\Sigma = \Sigma_\uparrow + \Sigma_\downarrow, \tag{A.4a}$$

$$\Sigma_s = \Sigma_\uparrow - \Sigma_\downarrow, \tag{A.4b}$$

$$P_\Sigma = \frac{\Sigma_s}{\Sigma}. \tag{A.4c}$$

The mismatch of the chemical potentials across the contact drives a current and spin current,

$$J^C_{\uparrow\downarrow} = \Sigma_{\uparrow\downarrow} \left(\mu^N_{\uparrow\downarrow} - \mu^F_{\uparrow\downarrow} \right)_c, \tag{A.5a}$$

$$J^C = J^C_\uparrow + J^C_\downarrow, \tag{A.5b}$$

$$J^C_s = J^C_\uparrow - J^C_\downarrow. \tag{A.5c}$$

The subscript c will always denote the function evaluated at the contact.

We will use the term current to refer to J, when in fact this is a particle current density. For constant J, the physical charge current I will be related to J by a relation $I = -AJ/e$ for some characteristic area A.

To reduce the number of subscripts and superscripts in the following, we adopt the notation for the potentials,

$$\begin{aligned} u &= \mu_s^N, \quad \varphi = \mu_s^F, \\ v &= \mu^N, \quad \psi = \mu^F, \end{aligned} \tag{A.6a}$$

and currents,

$$\begin{aligned} \jmath &= J_s, \\ J_c &= J^C, \\ \jmath_c &= J_s^C. \end{aligned} \tag{A.6b}$$

We rewrite equation (A.5) as

$$J_c = \Sigma\left(v_c - \psi_c\right) + \Sigma_s\left(u_c - \varphi_c\right), \tag{A.7a}$$

$$\jmath_c = \Sigma_s\left(v_c - \psi_c\right) + \Sigma\left(u_c - \varphi_c\right), \tag{A.7b}$$

and equations (A.2) and (A.3) as

$$\jmath = P_\sigma J + 4\frac{\sigma_\uparrow \sigma_\downarrow}{\sigma}\nabla\mu_s. \tag{A.8}$$

Using equations (A.4) and (A.7),

$$\jmath_c = P_\Sigma^i J_c + {R_C^i}^{-1}\left(u_c - \varphi_c\right), \tag{A.9}$$

where the contact resistance is

$$R_C^i = \frac{\Sigma^i}{4\Sigma_\uparrow^i \Sigma_\downarrow^i}. \tag{A.10}$$

The superscript i allows for contacts with difference conductances.

A.2 Boundary conditions

In this section we derive the relations between the potentials and the currents. This corresponds to the needed boundary conditions.

Semiconductor

For the semiconductor, $\sigma_{\uparrow}^{N} = \sigma_{\downarrow}^{N} = \sigma^{N}/2$, so $P_{\sigma}^{N} = 0$. Evaluating equation (A.8) at the contact gives

$$\jmath_{c}^{N} = \sigma^{N}(\nabla u)_{c}. \tag{A.11}$$

Ferromagnet

For the ferromagnet, one assumes μ_{s}^{F} satisfies the one dimensional diffusion equation. We choose the z' coordinate antiparallel to z with origin at the contact. The equation

$$\varphi''(z') - k_{F}^{2}\varphi(z') = 0, \tag{A.12}$$

with the boundary condition $\lim_{z'\to-\infty}\varphi(z') = 0$ has solution

$$\varphi(z') = \varphi_{c}e^{k_{F}z'}, \tag{A.13}$$

where $\varphi_{c} = \varphi(0)$ is a yet undetermined constant. Putting this into equation (A.8) and evaluating it at the contact gives

$$\jmath_{c}^{F} = P_{\sigma}^{F}J_{c}^{F} + R_{F}^{-1}\varphi_{c}, \tag{A.14}$$

where the ferromagnet resistance is

$$R_{F} = \frac{\sigma^{F}}{4\sigma_{\uparrow}^{F}\sigma_{\downarrow}^{F}k_{F}}. \tag{A.15}$$

Here, $\lambda_{F} = 1/k_{F}$ is the spin diffusion length in the ferromagnet.

Continuity assumptions

At the contact, the current and spin current are assumed continuous,

$$J_c = J_c^F = J_c^N, \tag{A.16a}$$

$$\jmath_c = \jmath_c^F = \jmath_c^N. \tag{A.16b}$$

Using equations (A.9), (A.14), and (A.16) we find the relation

$$\left(P_\sigma^F R_F + P_\Sigma^i R_C^i\right) J_c = \left(R_F + R_C^i\right) \jmath_c - u_c, \tag{A.17a}$$

and that φ_c is determined by

$$R_F^{-1}\varphi_c = \frac{\left(P_\Sigma^i - P_\sigma^F\right) R_C^i \jmath_c + P_\sigma^F u_c}{P_\sigma^F R_F + P_\Sigma^i R_C^i}. \tag{A.17b}$$

In the special case of zero current at the contact ($J_c = 0$), equation (A.17) reduces to

$$\jmath_c = \frac{1}{R_F + R_C^i} u_c, \tag{A.18a}$$

$$\varphi_c = \frac{R_F}{R_F + R_C^i} u_c. \tag{A.18b}$$

A.3 Nonlocal resistance

In this section we derive the precise relation between R_{NL} and $\mu_s^N(L)$. Note that we may write in general, for some $\bar{\mu}$,

$$\mu = \bar{\mu} + P_\sigma \mu_s, \tag{A.19}$$

and, following [28], define the voltage due to the difference in the chemical potentials across the contacts by

$$V_c = \left(\bar{\mu}_c^N - \bar{\mu}_c^F\right)/e. \tag{A.20}$$

We assume a fixed current $J_0 = |J_0| > 0$ flows down through the contact at $x = 0$ and to the left in the semiconductor for $x \leq 0$, and no current flows for $x > 0$. The experimentally measured quantity is the nonlocal resistance $R_{\mathrm{NL}} = V_L/I_0$, where $I_0 = -WLJ_0/e$ is the current through the contact at $x = 0$. It is convenient to introduce the effective nonlocal resistance $R_{\mathrm{NL}}^{\mathrm{SQ}}$ defined by

$$R_{\mathrm{NL}}^{\mathrm{SQ}} = WLR_{\mathrm{NL}} = -eV_L/J_0 = \frac{\bar{\mu}_c^F - \bar{\mu}_c^N}{J_0}. \tag{A.21}$$

To determine R_{NL}, we must express the difference of these chemical potentials in terms of $\mu_s^N(L)$.

Since there are two ferromagnetic contacts, we have separate functions ψ and φ for each contact which we will denote by ψ^0, φ^0, and ψ^L, φ^L. From equation (A.13), we have

$$\varphi^0\left(z'\right) = \varphi_0 e^{k_F z'}, \tag{A.22a}$$

$$\varphi^L\left(z'\right) = \varphi_L e^{k_F z'}. \tag{A.22b}$$

The physical restriction on the current flow in the semiconductor is imposed by noting that since $\sigma_s^N = 0$, equation (A.3b) gives $J^N = \sigma^N \nabla v$, so we must have

$$v_x(x) = \begin{cases} v_x(0) - \left(J_0/\sigma^N\right) x & \text{for } x \leq 0, \\ v_x(0) & \text{for } x > 0, \end{cases} \tag{A.23}$$

$v_y(x) = v_y(0)$, and $v_z(x) = v_z(0)$. Using equation (A.3b), the restriction on the current flow in each ferromagnet gives

$$\nabla\psi^0 = \left(J_0/\sigma^F\right) - P_\sigma^F \nabla\varphi^0, \tag{A.24a}$$

$$\nabla\psi^L = -P_\sigma^F \nabla\varphi^L. \tag{A.24b}$$

Integrating and enforcing $eV_c = v_x(0) - (\psi_c - P_\sigma^F \varphi_c)$,

$$\psi^0(z') = -eV_0 + P_\sigma^F \varphi_0 \left(2 - e^{k_F z'}\right) + v_x(0) + \left(J_0/\sigma^F\right) z', \tag{A.25a}$$

$$\psi^L(z') = -eV_L + P_\sigma^F \varphi_L \left(2 - e^{k_F z'}\right) + v_x(0). \tag{A.25b}$$

There is no current at the contact at $x = 0$, thus equation (A.7a) gives

$$\psi_L - v_L = P_\Sigma^L \left(u_L - \varphi_L\right), \tag{A.26}$$

and with equation (A.18b), we find

$$R_{\mathrm{NL}}^{\mathrm{SQ}} = (\psi_L - v_L) - P_\sigma^F \varphi_L = \left[P_\Sigma^L \left(1 - \frac{R_F}{R_F + R_C^L}\right) - \frac{P_\sigma^F R_F}{R_F + R_C^L}\right] \frac{u_x(L)}{J_0}. \tag{A.27}$$

A.4 Diffusion equation

In this section we show how to solve for $\mu_s^N(L)$. This method is based on the one described in [24]. Inside the semiconductor, u satisfies the diffusion equation,

$$D\nabla^2 u - \frac{u}{\tau} + \omega \times u = 0. \tag{A.28}$$

Here, D is the diffusion constant, τ the spin lifetime, and $\omega = (g\mu_B/\hbar)\, B$ is proportional to the applied magnetic field (with g the gyromagnetic ratio and μ_B the Bohr magneton). The spin diffusion length in the semiconductor is $\lambda = 1/k = \sqrt{D\tau}$.

The function $u = u(x)$ only varies along x, and we introduce the notation

$$u_x(x) = \begin{cases} u_{x-}(x) \text{ for } x < 0, \\ u_{x0}(x) \text{ for } 0 \leq x \leq L, \\ u_{x+}(x) \text{ for } L < x, \end{cases} \tag{A.29}$$

with similar expressions for u_y and u_z. The most general solution to equation (A.28) decouples u_z from u_x and u_y. The requirement $\lim_{x\to\pm\infty} u(x) = 0$ yields

$$u_{z\pm}(x) = A^{\mp} e^{\mp kx}, \tag{A.30a}$$

$$u_{z0}(x) = A_0^{+} e^{kx} + A_0^{-} e^{-kx}, \tag{A.30b}$$

and

$$u_{x\pm}(x) = B^{\mp} e^{\mp\kappa x} + C^{\mp} e^{\mp\bar{\kappa} x}, \tag{A.31a}$$

$$u_{y\pm}(x) = iB^{\mp} e^{\mp\kappa x} - iC^{\mp} e^{\mp\bar{\kappa} x}, \tag{A.31b}$$

$$u_{x0}(x) = B_0^{+} e^{\kappa x} + B_0^{-} e^{-\kappa x} + C_0^{+} e^{\bar{\kappa} x} + C_0^{-} e^{-\bar{\kappa} x}, \tag{A.31c}$$

$$u_{y0}(x) = iB_0^{+} e^{\kappa x} + iB_0^{-} e^{-\kappa x} - iC_0^{+} e^{\bar{\kappa} x} - iC_0^{-} e^{-\bar{\kappa} x}, \tag{A.31d}$$

where $\kappa = k\sqrt{1 + i\omega\tau}$. The twelve constants A, B and C (with their various subscripts and superscripts) must be determined by imposing the appropriate boundary conditions.

We first require u be continuous at $x = 0$ and $x = L$; this gives six equations. We now require a boundary condition on ∇u, but ∇u cannot be assumed continuous at the contact. We make the assumption that the total spin current at the contact is the sum of the spin currents on either side, i.e.,

$$\jmath_0 = \sigma^N \left[-u_-'(0) + u_0'(0)\right], \tag{A.32a}$$

$$\jmath_L = \sigma^N \left[-u_0'(L) + u_+'(L)\right]. \tag{A.32b}$$

The signs have been chosen to be consistent with the physical geometry. The only nonzero component of the current at the contacts inside the semiconductor is the x component at $x = 0$, so we use equation (A.17a). For all other components there

is zero current at the contact, and we use equation (A.18a). Together with equation (A.32), this gives the other six equations,

$$-u'_{z-}(0) + u'_{z0}(0) + \eta_0 u_z(0) = 0, \tag{A.33a}$$

$$u'_{z+}(L) - u'_{z0}(L) + \eta_L u_z(L) = 0, \tag{A.33b}$$

$$-u'_{x-}(0) + u'_{x0}(0) + \eta_0 u_x(0) = \Delta, \tag{A.33c}$$

$$u'_{x+}(L) - u'_{x0}(L) + \eta_L u_x(L) = 0, \tag{A.33d}$$

$$-u'_{y-}(0) + u'_{y0}(0) + \eta_0 u_y(0) = 0, \tag{A.33e}$$

$$u'_{y+}(L) - u'_{y0}(L) + \eta_L u_y(L) = 0, \tag{A.33f}$$

where

$$\eta_i^{-1} = -\sigma^N \left(R_F + R_C^i\right), \tag{A.34a}$$

$$\Delta = -(-J_0)\left(P_\sigma^F R_F + P_\Sigma^0 R_C^0\right)\eta_0. \tag{A.34b}$$

We define the r-parameter, $r_i = -\eta_i^{-1}$, introduced in equation (2.5).

These equations can be organized into a matrix equation and solved algebraically. A solution for u_z corresponds to a condition of vanishing determinant,

$$e^{-2L/\lambda} = \left(1 + \frac{2r_0}{\lambda}\right)\left(1 + \frac{2r_L}{\lambda}\right), \tag{A.35}$$

which can never be satisfied,[1] thus $u_z = 0$ is the only allowed solution. The other two components form an eight dimensional linear system. Solving this gives the remaining constants, and thus $u_x(L) = e^{-\kappa L}B^- + e^{-\bar{\kappa}L}C^-$.

[1]Except at the nonphysical point $L/\lambda = r_i/\lambda = 0$.

Finally, by using $p_1 = -\sigma^N \Delta / J_0$ along with equation (A.27), we can introduce R_{SQ} from equation (2.6) and the polarizations

$$p_1 = \frac{P_\sigma^F R_F + P_\Sigma^L R_C^L}{R_F + R_C^L}, \tag{A.36a}$$

$$p_2/p_1 = \left(1 - \frac{P_\sigma^F R_F}{P_\Sigma^L R_C^L}\right) \Bigg/ \left(1 + \frac{P_\sigma^F R_F}{P_\Sigma^L R_C^L}\right), \tag{A.36b}$$

to write

$$\frac{R_{\mathrm{NL}}^{\mathrm{SQ}}}{R_{\mathrm{SQ}}} = \frac{p_1 p_2}{W/\lambda} \left[-\frac{k u_x(L)}{\Delta}\right]. \tag{A.37}$$

The factor in brackets is the function f given in equation (2.4).

Appendix B

Tight-Binding Model

In this appendix, we review the assumptions of the tight-binding model as derived from Bloch's theorem. We denote the position and momentum operators respectively by $\mathbf{Q}$ and $\mathbf{P}$.

B.1 Transition operators

We first define the position-space translation operator, $T(\mathbf{r}) = e^{-i\mathbf{r}\cdot\mathbf{P}}$, and the momentum-space translation operator, $T_{\mathbf{k}} = e^{-i\mathbf{k}\cdot\mathbf{Q}}$. We assume zero magnetic field.[1] Each has a simple inverse: $T^{-1}(\mathbf{r}) = T(-\mathbf{r})$ and $T_{\mathbf{k}}^{-1} = T_{-\mathbf{k}}$. We also note the derivatives: $\nabla_{\mathbf{k}} T_{\mathbf{k}} = -i\mathbf{Q}T_{\mathbf{k}}$ and $\nabla_{\mathbf{k}} T_{\mathbf{k}}^{-1} = i\mathbf{Q}T_{\mathbf{k}}^{-1}$.

We can compute a useful commutation relation of these translations operators.

[1] For nonzero field, much of the following can be recast in terms of the magnetic translation operators [70].

Application of the Baker–Campbell–Hausdorff formula gives

$$T(\mathbf{r})\,T_{\mathbf{k}} = e^{-i(\mathbf{r}\cdot\mathbf{P}+\mathbf{k}\cdot\mathbf{Q})-\frac{1}{2}[\mathbf{r}\cdot\mathbf{P},\mathbf{k}\cdot\mathbf{Q}]}, \tag{B.1a}$$

$$T_{\mathbf{k}}T(\mathbf{r}) = e^{-i(\mathbf{r}\cdot\mathbf{P}+\mathbf{k}\cdot\mathbf{Q})+\frac{1}{2}[\mathbf{r}\cdot\mathbf{P},\mathbf{k}\cdot\mathbf{Q}]}. \tag{B.1b}$$

Only a single commutator appears above since $[\mathbf{r}\cdot\mathbf{P},\mathbf{k}\cdot\mathbf{Q}] = -i\mathbf{r}\cdot\mathbf{k}$. Substituting this gives

$$T(\mathbf{r})\,T_{\mathbf{k}} = e^{-i\mathbf{r}\cdot\mathbf{k}}T_{\mathbf{k}}T(\mathbf{r})\,. \tag{B.2}$$

B.2 Bloch Hamiltonian

Given a Hamiltonian H and a set of N lattice vectors $\{\mathbf{R}_n^0\}$ such that the Hamiltonian commutes with each $T(\mathbf{R}_n^0)$, we may choose a set of common eigenvectors according to Bloch's theorem,

$$H\,|\psi_{n\mathbf{k}}\rangle = E_{n\mathbf{k}}\,|\psi_{n\mathbf{k}}\rangle\,, \tag{B.3a}$$

$$T(\mathbf{R}_m^0)\,|\psi_{n\mathbf{k}}\rangle = e^{-i\mathbf{k}\cdot\mathbf{R}_m^0}\,|\psi_{n\mathbf{k}}\rangle\,. \tag{B.3b}$$

Given periodic boundary conditions, the set of allowed $\mathbf{k}$ becomes countable and may be restricted to the first Brillouin zone due to the periodicity of the eigenvalues with respect to translation by a reciprocal lattice vector $\mathbf{G}$. For each $\mathbf{k}$, the transformation $|u_{n\mathbf{k}}\rangle = T_{\mathbf{k}}\,|\psi_{n\mathbf{k}}\rangle$ gives a set of states which are invariant under lattice translations, i.e., using equation (B.2), $T(\mathbf{R}_m^0)\,|u_{n\mathbf{k}}\rangle = |u_{n\mathbf{k}}\rangle$. A general operator then transforms according to $A_{\mathbf{k}} = T_{\mathbf{k}}AT_{\mathbf{k}}^{-1}$. Note that the derivative of a transformed operator may be computed as

$$\nabla_{\mathbf{k}}A_{\mathbf{k}} = \nabla_{\mathbf{k}}\left(T_{\mathbf{k}}AT_{\mathbf{k}}^{-1}\right) = i\,[A_{\mathbf{k}},\mathbf{Q}]\,. \tag{B.4}$$

B.3 Tight-binding approximation

In the tight biding model, one assumes there exists a finite set $\{|\varphi_\nu\rangle\}$ of relevant atomic orbitals. The corresponding Bloch orbital states,

$$|\phi_{\nu\mathbf{k}}\rangle = \frac{1}{\sqrt{N}} \sum_{n=1}^{N} e^{i\mathbf{k}\cdot\mathbf{R}_n^0} T\left(\mathbf{R}_n^0\right) |\varphi_\nu\rangle\,, \tag{B.5}$$

provide a complete bases for the space of Bloch eigenstates $\{|\psi_{n\mathbf{k}}\rangle\}$, i.e.,

$$|\psi_{n\mathbf{k}}\rangle = \sum_{\nu} M_{\mathbf{k}}^{\nu n} |\phi_{\nu\mathbf{k}}\rangle\,, \tag{B.6a}$$

$$|\phi_{\nu\mathbf{k}}\rangle = \sum_{n} W_{\mathbf{k}}^{n\nu} |\psi_{n\mathbf{k}}\rangle\,, \tag{B.6b}$$

with $M_{\mathbf{k}}^{\nu n} = \bar{W}_{\mathbf{k}}^{\nu n}$. The second overlap term in

$$\langle \phi_{\nu'\mathbf{k}} \,|\, \phi_{\nu\mathbf{k}} \rangle = \langle \varphi_{\nu'} \,|\, \varphi_\nu \rangle + \sum_{\mathbf{R}_n^0 \neq 0}^{N} e^{i\mathbf{k}\cdot\mathbf{R}_n^0} \left\langle \varphi_{\nu'} \,\middle|\, T\left(\mathbf{R}_n^0\right) \,\middle|\, \varphi_\nu \right\rangle \tag{B.7}$$

is small, thus the states $\{|\varphi_\nu\rangle\}$ are assumed formally orthonormal.

Since each $|\phi_{nk}\rangle$ satisfies

$$T\left(\mathbf{R}_m^0\right) |\phi_{\nu\mathbf{k}}\rangle = e^{-i\mathbf{k}\cdot\mathbf{R}_m^0} |\phi_{\nu\mathbf{k}}\rangle\,, \tag{B.8}$$

the transformed orbital states $|v_{n\mathbf{k}}\rangle = T_{\mathbf{k}} |\phi_{nk}\rangle$ are invariant under lattice translations. One typically knows the matrix elements of an effective Hamiltonian in the bases of these periodic Bloch orbitals,

$$H_{\mathbf{k}}^{\nu\nu'} = \langle v_{\nu\mathbf{k}} \,|\, H_{\mathbf{k}} \,|\, v_{\nu'\mathbf{k}} \rangle = \sum_{n} \bar{W}_{\mathbf{k}}^{n\nu} E_{n\mathbf{k}} W_{\mathbf{k}}^{n\nu'}, \tag{B.9}$$

which determines the coefficients $M_{\mathbf{k}}^{\nu n}$.

Appendix C

Many-Body Interaction

The BCS theory of superconductivity is often introduced as a consequence of the effective electron-electron interaction arising from the underlying electron-phonon interaction. In this appendix, we review general two-particle interactions, and derive the form of the electron-electron interaction when applied to the tight-binding model. These results are the foundation for deriving the intrinsic TMD superconducting state.

C.1 Electron-electron interaction

Consider a general spin-independent interaction potential $v(\mathbf{x}, \mathbf{x}')$ which depends on the positions $\mathbf{x}$ and $\mathbf{x}'$ of a pair of particles [71]. In a multiparticle system of dimension d with no self-interaction, the interaction V may be written as an additive

pair operator in a given bases, $C_\alpha^\dagger |0\rangle = |\alpha\rangle = |f_\alpha\rangle \otimes |\sigma_\alpha\rangle$, of fermionic Fock operators,

$$\begin{aligned} V &= \frac{1}{2} \sum_{i \neq j} v\left(\mathbf{Q}_i, \mathbf{Q}_j\right), \\ &= \frac{1}{4} \sum_{\alpha,\beta,\delta,\gamma} \langle \alpha\beta \,|\, v \,|\, \gamma\delta \rangle \, C_\alpha^\dagger C_\beta^\dagger C_\delta C_\gamma, \\ &= \frac{1}{2} \sum_{\alpha,\beta,\delta,\gamma} v_{\alpha\beta,\gamma\delta} C_\alpha^\dagger C_\beta^\dagger C_\delta C_\gamma. \end{aligned} \tag{C.1}$$

Here, $|\alpha\beta\rangle = \left(|\alpha\rangle\,|\beta\rangle - |\beta\rangle\,|\alpha\rangle\right)/\sqrt{2}$, and we introduce the symbol

$$\begin{aligned} v_{\alpha\beta,\gamma\delta} &= \left(\langle f_\alpha| \left\langle f_\beta\right|\right) v \left(\left|f_\gamma\right\rangle \left|f_\delta\right\rangle\right) \left\langle \sigma_\alpha \,|\, \sigma_\gamma \right\rangle \left\langle \sigma_\beta \,|\, \sigma_\delta \right\rangle, \\ &= \delta_{\sigma_\alpha \sigma_\gamma} \delta_{\sigma_\beta \sigma_\delta} \int \bar{f}_\alpha\left(\mathbf{x}\right) \bar{f}_\beta\left(\mathbf{x}'\right) v\left(\mathbf{x}, \mathbf{x}'\right) f_\gamma\left(\mathbf{x}\right) f_\delta\left(\mathbf{x}'\right) \mathrm{d}^d\mathbf{x}\, \mathrm{d}^d\mathbf{x}', \end{aligned} \tag{C.2}$$

so that $\langle \alpha\beta \,|\, v \,|\, \gamma\delta \rangle = v_{\alpha\beta,\gamma\delta} - v_{\alpha\beta,\delta\gamma}$. For a given interaction, the explicit form of V depends on the choice of basis states. For illustration, we consider the position and momentum space descriptions below.

If one chooses the continuous basis of position eigenstates, $\Psi_\sigma^\dagger\left(\mathbf{x}\right)|0\rangle = |\mathbf{x}\rangle \otimes |\sigma\rangle$, then equation (C.1) takes the form of an integral over density-density interactions,

$$V = \frac{1}{2} \int v\left(\mathbf{x}, \mathbf{x}'\right) {:}\rho\left(\mathbf{x}\right) \rho\left(\mathbf{x}'\right){:}\, \mathrm{d}^d\mathbf{x}\, \mathrm{d}^d\mathbf{x}', \tag{C.3}$$

where the colon denotes normal ordering and

$$\rho\left(\mathbf{x}\right) = \sum_\sigma \Psi_\sigma^\dagger\left(\mathbf{x}\right) \Psi_\sigma\left(\mathbf{x}\right). \tag{C.4}$$

For interactions $v\left(\mathbf{r}\right)$ which depend only on the relative separation, $\mathbf{r} = \mathbf{x}' - \mathbf{x}$, if one chooses the countable basis of box normalized momentum eigenstates in a volume Ω with periodic boundary conditions, $c_{\mathbf{p}\sigma}^\dagger |0\rangle = |\mathbf{p}\rangle \otimes |\sigma\rangle$, with $\langle \mathbf{x} \,|\, \mathbf{p} \rangle = \Omega^{-1/2} e^{i\mathbf{p}\cdot\mathbf{x}}$, then

$$V = \frac{1}{2} \sum_{\mathbf{p},\mathbf{p}',\mathbf{q}} \sum_{\sigma,\sigma'} \tilde{v}_\mathbf{q} c_{\mathbf{p}+\mathbf{q}\sigma}^\dagger c_{\mathbf{p}'-\mathbf{q}\sigma'}^\dagger c_{\mathbf{p}'\sigma'} c_{\mathbf{p}\sigma}, \tag{C.5}$$

where

$$\tilde{v}_{\mathbf{q}} = \frac{1}{\Omega} \int v(\mathbf{r})\, e^{-i\mathbf{q}\cdot\mathbf{r}}\, \mathrm{d}^d\mathbf{r}. \tag{C.6}$$

Interaction in the tight-binding model

We now apply the above to the basis introduced in the tight-binding model. Introduce a Wannier representation,

$$|\phi_{\nu\mathbf{k}}\rangle = \frac{1}{\sqrt{N}} \sum_{\mathbf{R}} e^{i\mathbf{k}\cdot\mathbf{R}}\, |\phi_{\nu\mathbf{R}}\rangle\,, \tag{C.7}$$

where for convenience we write $\mathbf{R}$ for $\mathbf{R}_n^0$. We adopt the following section-specific notation for the Fock operators,

$$a^\dagger_{\mathbf{k}\nu\sigma}\,|0\rangle = |\phi_{\nu\mathbf{k}\sigma}\rangle\ = |\phi_{\nu\mathbf{k}}\rangle \otimes |\sigma\rangle\,, \tag{C.8a}$$

$$a^\dagger_{\mathbf{R}\nu\sigma}\,|0\rangle = |\phi_{\nu\mathbf{R}\sigma}\rangle = |\phi_{\nu\mathbf{R}}\rangle \otimes |\sigma\rangle\,, \tag{C.8b}$$

which explicitly separates out the spin index. Since

$$\langle \mathbf{x}\,|\,\phi_{\nu\mathbf{R}}\rangle = \langle \mathbf{x}-\mathbf{R}\,|\,\varphi_\nu\rangle = \varphi_\nu(\mathbf{x}-\mathbf{R})\,, \tag{C.9}$$

by keeping only on-center, like-orbital terms, the interaction may by simplified to the approximate form

$$V \backsimeq \frac{1}{2} \sum_{\mathbf{R},\mathbf{R}'} \sum_{\nu,\nu'} v^{\nu\nu'}_{\mathbf{R}\mathbf{R}'} {:}\, n_{\mathbf{R}\nu} n_{\mathbf{R}'\nu'} \,{:}, \tag{C.10}$$

with the number operators,

$$n_{\nu\mathbf{R}} = \sum_\sigma a^\dagger_{\mathbf{R}\nu\sigma} a_{\mathbf{R}\nu\sigma}, \tag{C.11}$$

and interaction integral,

$$v^{\nu\nu'}_{\mathbf{R}\mathbf{R}'} = \int v(\mathbf{x},\mathbf{x}')\, |\varphi_\nu(\mathbf{x}-\mathbf{R})|^2 |\varphi_{\nu'}(\mathbf{x}'-\mathbf{R}')|^2\, \mathrm{d}^d\mathbf{x}\, \mathrm{d}^d\mathbf{x}'. \tag{C.12}$$

This sum over density-density interactions mimics equation (C.3).

Further, assuming that the interaction depends only on the relative separation, $v^{\nu\nu'}_{\mathbf{R}\mathbf{R}'} = v_{\nu\nu'}\left(\mathbf{R}' - \mathbf{R}\right)$, we may introduce the Fourier expansion

$$\tilde{v}^{\nu\nu'}_{\mathbf{q}} = \sum_{\mathbf{R}} v_{\nu\nu'}\left(\mathbf{R}\right) e^{i\mathbf{q}\cdot\mathbf{R}}, \tag{C.13}$$

and switch back to the Bloch representation,

$$V = \frac{1}{2}\left(\frac{\Omega}{N}\right)^2 \sum_{\nu,\nu'} \sum_{\sigma,\sigma'} \sum_{\mathbf{k}',\bar{\mathbf{k}}} \sum_{\mathbf{k},\bar{\mathbf{k}}'} \sum_{\mathbf{q}} \tilde{v}^{\nu\nu'}_{\mathbf{q}} \\ \delta\left[\mathbf{q} - \left(\mathbf{k} - \bar{\mathbf{k}}\right)\right] \delta\left[\mathbf{q} - \left(\bar{\mathbf{k}}' - \mathbf{k}'\right)\right] a^\dagger_{\mathbf{k}\nu\sigma} a^\dagger_{\bar{\mathbf{k}}'\nu'\sigma'} a_{\mathbf{k}'\nu'\sigma'} a_{\mathbf{k}\nu\sigma}. \tag{C.14}$$

As a convenience, we have written this as a sum over a countable set of momentum states, however any sum over momentum may be converted to an integral according to the substitution $\sum_{\mathbf{k}} \to (N/\Omega) \int \mathrm{d}^d\mathbf{k}$. Using this, we may integrate out the δ-functions and obtain a form that mimics equation (C.5),

$$V = \frac{1}{2} \sum_{\mathbf{k},\mathbf{k}',\mathbf{q}} \sum_{\nu,\nu'} \sum_{\sigma,\sigma'} \tilde{v}^{\nu\nu'}_{\mathbf{q}} a^\dagger_{\mathbf{k}+\mathbf{q}\nu\sigma} a^\dagger_{\mathbf{k}'-\mathbf{q}\nu'\sigma'} a_{\mathbf{k}'\nu'\sigma'} a_{\mathbf{k}\nu\sigma}. \tag{C.15}$$

Appendix D

Intrinsic Superconducting Phases

D.1 Interaction in the effective model

Note that for the effective low-energy, dual-valley model, equation (C.15) is oversimplified. We must first split up each integral into a region about each valley center. The allowed transitions are still constrained by global conservation of momentum.

Starting with equation (C.14), the integral over $\mathbf{q}$ is unchanged,

$$V = \frac{1}{2}\frac{\Omega}{N}\sum_{\substack{\nu,\nu'\\ \sigma,\sigma'}}\sum_{\mathbf{k}',\bar{\mathbf{k}}}\sum_{\mathbf{k},\bar{\mathbf{k}}'}\tilde{v}^{\nu\nu'}_{\mathbf{k}-\bar{\mathbf{k}}}\delta\left[\left(\bar{\mathbf{k}}'-\mathbf{k}'\right)-\left(\mathbf{k}-\bar{\mathbf{k}}\right)\right]a^{\dagger}_{\bar{\mathbf{k}}\nu\sigma}a^{\dagger}_{\bar{\mathbf{k}}'\nu'\sigma'}a_{\mathbf{k}'\nu'\sigma'}a_{\mathbf{k}\nu\sigma}. \quad \text{(D.1)}$$

We now split up the integral over the global momentum coordinates into integrals over relative coordinates centered about each valley; this introduces an additional overall factor of 2^{-4} (two valley centers per momentum integral with four independent momentum-space coordinates). We then restrict each integral to a suitable region about each valley (indicated by a prime on the summation). The relative coordinates are thus introduced by the substitution $\mathbf{k} \to \mathbf{k} + \tau\mathbf{K}$.

Global conservation of momentum, represented by the δ-function, now requires

$$\mathbf{k} - \bar{\mathbf{k}} + (\tau - \bar{\tau})\,\mathbf{K} = \bar{\mathbf{k}}' - \mathbf{k}' + (\bar{\tau}' - \tau')\,\mathbf{K}. \tag{D.2}$$

Since $|\mathbf{k}| \ll |\mathbf{K}|$, the above is actually the two independent conditions,

$$\mathbf{k} - \bar{\mathbf{k}} = \bar{\mathbf{k}}' - \mathbf{k}', \tag{D.3a}$$

$$\tau - \bar{\tau} = \bar{\tau}' - \tau'. \tag{D.3b}$$

There are three allowed cases for the sum over the valley indexes: intravalley scattering with $\tau = \bar{\tau}$ and $\tau' = \bar{\tau}'$; intervalley scattering with $\tau = -\tau'$ and $\bar{\tau} = -\bar{\tau}'$; and exchange with $\tau = \bar{\tau}'$ and $\bar{\tau} = \tau'$. We indicate summation over the allowed cases by adding a prime to the sum. Thus, we obtain

$$V = \frac{1}{2^5} \sum_{\mathbf{k},\mathbf{k}',\mathbf{q}}{}' \sum_{\substack{\nu,\nu' \\ \sigma,\sigma'}} \sum_{\substack{\tau,\bar{\tau}, \\ \tau',\bar{\tau}'}}{}' \tilde{v}^{\nu'\nu}_{\mathbf{q}+(\bar{\tau}-\tau)\mathbf{K}} a^{\nu}_{\bar{\tau}\sigma}{}^{\dagger}(\mathbf{k}+\mathbf{q})\, a^{\nu'}_{\bar{\tau}'\sigma'}{}^{\dagger}(\mathbf{k}'-\mathbf{q})\, a^{\nu'}_{\tau'\sigma'}(\mathbf{k}')\, a^{\nu}_{\tau\sigma}(\mathbf{k})\,. \tag{D.4}$$

The expected BCS instability is strongest for scattering with $\mathbf{k} = -\mathbf{k}'$. Restricting the sum over $\mathbf{k}'$ to this condition, relabeling the momentum indexes, and defining $v^{\nu\nu'}_{\mathbf{q}} = 2^{-4}\tilde{v}^{\nu'\nu}_{\mathbf{q}}$ gives

$$V = \frac{1}{2} \sum_{\mathbf{k},\mathbf{k}'}{}' \sum_{\substack{\nu,\nu' \\ \sigma,\sigma'}} \sum_{\substack{\tau,\bar{\tau}, \\ \tau',\bar{\tau}'}}{}' v^{\nu\nu'}_{\mathbf{k}'-\mathbf{k}+(\bar{\tau}-\tau)\mathbf{K}} a^{\nu}_{\bar{\tau}\sigma}{}^{\dagger}(\mathbf{k}')\, a^{\nu'}_{\bar{\tau}'\sigma'}{}^{\dagger}(-\mathbf{k}')\, a^{\nu'}_{\tau'\sigma'}(-\mathbf{k})\, a^{\nu}_{\tau\sigma}(\mathbf{k})\,. \tag{D.5}$$

Expanding the sum over the valley indexes gives

$$V = \frac{1}{2} \sum_{\mathbf{k},\mathbf{k}'}{}' \sum_{\tau,\tau',} \sum_{\nu,\nu'} \sum_{\sigma,\sigma'} \Big[v^{\nu\nu'}_{\mathbf{k}'-\mathbf{k}} a^{\nu}_{\tau\sigma}{}^{\dagger}(\mathbf{k}')\, a^{\nu'}_{\tau'\sigma'}{}^{\dagger}(-\mathbf{k}')\, a^{\nu'}_{\tau'\sigma'}(-\mathbf{k})\, a^{\nu}_{\tau\sigma}(\mathbf{k}) \tag{D.6a}$$

$$+ v^{\nu\nu'}_{\mathbf{k}'-\mathbf{k}+(\tau'-\tau)\mathbf{K}} a^{\nu}_{\tau'\sigma}{}^{\dagger}(\mathbf{k}')\, a^{\nu'}_{-\tau'\sigma'}{}^{\dagger}(-\mathbf{k}')\, a^{\nu'}_{-\tau\sigma'}(-\mathbf{k})\, a^{\nu}_{\tau\sigma}(\mathbf{k}) \tag{D.6b}$$

$$+ v^{\nu\nu'}_{\mathbf{k}'-\mathbf{k}+(\tau'-\tau)\mathbf{K}} a^{\nu}_{\tau'\sigma}{}^{\dagger}(\mathbf{k}')\, a^{\nu'}_{\tau\sigma'}{}^{\dagger}(-\mathbf{k}')\, a^{\nu'}_{\tau'\sigma'}(-\mathbf{k})\, a^{\nu}_{\tau\sigma}(\mathbf{k}) \Big]. \tag{D.6c}$$

Projecting to bands with $\alpha = \tau = \sigma$,

$$V = \frac{1}{2}{\sum_{\mathbf{k},\mathbf{k}'}}' \sum_{\nu,\nu'} \sum_{\alpha} v^{\nu\nu'}_{\mathbf{k}'-\mathbf{k}} \Big[a^{\nu\,\dagger}_{\alpha}(\mathbf{k}')\, a^{\nu'\,\dagger}_{\alpha}(-\mathbf{k}')\, a^{\nu'}_{\alpha}(-\mathbf{k})\, a^{\nu}_{\alpha}(\mathbf{k}) \tag{D.7a}$$

$$+ a^{\nu\,\dagger}_{\alpha}(\mathbf{k}')\, a^{\nu'\,\dagger}_{-\alpha}(-\mathbf{k}')\, a^{\nu'}_{-\alpha}(-\mathbf{k})\, a^{\nu}_{\alpha}(\mathbf{k}) \tag{D.7b}$$

$$+ \sum_{\alpha'} a^{\nu\,\dagger}_{\alpha}(\mathbf{k}')\, a^{\nu'\,\dagger}_{\alpha'}(-\mathbf{k}')\, a^{\nu'}_{\alpha'}(-\mathbf{k})\, a^{\nu}_{\alpha}(\mathbf{k}) \Big]. \tag{D.7c}$$

This simplifies into explicit intervalley and intravalley terms,

$$V = {\sum_{\mathbf{k},\mathbf{k}'}}' \sum_{\nu,\nu'} \sum_{\alpha} v^{\nu\nu'}_{\mathbf{k}'-\mathbf{k}} \Big[a^{\nu\,\dagger}_{\alpha}(\mathbf{k}')\, a^{\nu'\,\dagger}_{\alpha}(-\mathbf{k}')\, a^{\nu'}_{\alpha}(-\mathbf{k})\, a^{\nu}_{\alpha}(\mathbf{k}) + a^{\nu\,\dagger}_{\alpha}(\mathbf{k}')\, a^{\nu'\,\dagger}_{-\alpha}(-\mathbf{k}')\, a^{\nu'}_{-\alpha}(-\mathbf{k})\, a^{\nu}_{\alpha}(\mathbf{k}) \Big]. \tag{D.8}$$

D.2 Superconducting channels

Assuming the interaction is real-valued and orbital-independent,[1]

$$v^{\nu\nu'}_{\mathbf{k}'-\mathbf{k}} = v(\mathbf{k}'-\mathbf{k}) = v(\mathbf{k}-\mathbf{k}'), \tag{D.9}$$

equation (D.8) projected to the upper $n=-1$ bands with $\tau=\sigma$ is

$$P^{n=-}_{\tau=\sigma}(H^V) = \sum_{\mathbf{k},\mathbf{k}'} v(\mathbf{k}'-\mathbf{k}) \Big(2|A_{\mathbf{k}\mathbf{k}'}|^2 c^{\dagger}_{\mathbf{k}'\uparrow} c^{\dagger}_{-\mathbf{k}'\downarrow} c_{-\mathbf{k}\downarrow} c_{\mathbf{k}\uparrow} + A^2_{\mathbf{k}\mathbf{k}'} c^{\dagger}_{\mathbf{k}'\uparrow} c^{\dagger}_{-\mathbf{k}'\uparrow} c_{-\mathbf{k}\uparrow} c_{\mathbf{k}\uparrow} + A^2_{\mathbf{k}'\mathbf{k}} c^{\dagger}_{\mathbf{k}'\downarrow} c^{\dagger}_{-\mathbf{k}'\downarrow} c_{-\mathbf{k}\downarrow} c_{\mathbf{k}\downarrow} \Big), \tag{D.10}$$

where

$$A_{\mathbf{k}\mathbf{k}'} = e^{i(\phi_{\mathbf{k}'}-\phi_{\mathbf{k}})} \sin\frac{\theta_{\mathbf{k}'}}{2} \sin\frac{\theta_{\mathbf{k}}}{2} + \cos\frac{\theta_{\mathbf{k}'}}{2} \cos\frac{\theta_{\mathbf{k}}}{2}. \tag{D.11}$$

[1] As noted in section 3.3, this choice forbids the intravalley pairing. However, for the complex-valued case, only the intravalley pairing term survives. For completeness, we still consider the intravalley terms in this appendix.

For the intravalley channels, the coefficient can be expanded as

$$A^2_{\mathbf{k}\mathbf{k}'} = \sum_{m=0}^{2} \bar{f}^m_{\mathbf{k}} \cdot g^m_{\mathbf{k}'}, \tag{D.12}$$

with $f^m_{\mathbf{k}} = g^m_{\mathbf{k}'}$ and

$$f^0_{\mathbf{k}} = \cos^2 \frac{\theta_{\mathbf{k}}}{2} = \frac{1}{2} P_0 \left(\cos\theta_{\mathbf{k}}\right) + \frac{1}{2} P_1 \left(\cos\theta_{\mathbf{k}}\right), \tag{D.13a}$$

$$e^{-i\phi_{\mathbf{k}}} f^1_{\mathbf{k}} = \sqrt{2} \sin \frac{\theta_{\mathbf{k}}}{2} \cos \frac{\theta_{\mathbf{k}}}{2} = \frac{1}{\sqrt{2}} P_1 \left(\sin\theta_{\mathbf{k}}\right), \tag{D.13b}$$

$$e^{-2i\phi_{\mathbf{k}}} f^2_{\mathbf{k}} = \sin^2 \frac{\theta_{\mathbf{k}}}{2} = \frac{1}{2} P_0 \left(\cos\theta_{\mathbf{k}}\right) - \frac{1}{2} P_1 \left(\cos\theta_{\mathbf{k}}\right). \tag{D.13c}$$

Here, P_l are the Legendre polynomials: $P_0(x) = 1$ and $P_1(x) = x$.

For the intervalley channels, the coefficient can be expanded as

$$2|A_{\mathbf{k}\mathbf{k}'}|^2 = \sum_{l=0}^{1} \bar{f}^l_{\mathbf{k}} \cdot g^l_{\mathbf{k}'} + \bar{f}_{\mathbf{k}} \cdot g_{\mathbf{k}'}, \tag{D.14}$$

with $f^l_{\mathbf{k}} = g^l_{\mathbf{k}'}$, $f_{\mathbf{k}} = g_{\mathbf{k}'}$, and

$$f^0_{\mathbf{k}} = \sqrt{2} P_0 \left(\cos\theta_{\mathbf{k}}\right), \tag{D.15a}$$

$$f^1_{\mathbf{k}} = \sqrt{2} P_1 \left(\cos\theta_{\mathbf{k}}\right), \tag{D.15b}$$

$$f_{\mathbf{k}} = \sqrt{2} P_1 \left(\sin\theta_{\mathbf{k}}\right) \hat{\mathbf{k}}. \tag{D.15c}$$

Mean field approximation

Using the mean field approximation, we make replacements of the form $AB = A\langle B\rangle + \langle A\rangle B - \langle A\rangle\langle B\rangle$, where A (B) is the product of two creation (annihilation) operators. The expectation value is taken in the superconducting ground state. We assume $v(\mathbf{k} - \mathbf{k}') = -v_0$ is a constant attractive interaction, possibly with some effective interaction range which further restricts the summation. Equation (D.10)

thus reduces to a sum of terms of the form

$$-\sum_{\mathbf{k}}\left(\bar{\Delta}_{\mathbf{k}}^{\gamma\gamma'}c_{-\mathbf{k}\gamma'}c_{\mathbf{k}\gamma}+\frac{\varepsilon_{\gamma\gamma'}}{2}\right)+\text{h.c.}, \tag{D.16}$$

where $\gamma=\gamma'=\pm1$ ($\gamma=-\gamma'=1$) corresponds to the intravalley (intervalley) scattering channels,

$$\Delta_{\mathbf{k}}^{\gamma\gamma'}=-{\sum_{\mathbf{k}'}}'\,\bar{v}_{\mathbf{k}\mathbf{k}'}^{\gamma\gamma'}\left\langle c_{-\mathbf{k}'\gamma'}c_{\mathbf{k}'\gamma}\right\rangle, \tag{D.17}$$

and

$$\varepsilon_{\gamma\gamma'}=-\sum_{\mathbf{k},\mathbf{k}'}v_{\mathbf{k}\mathbf{k}'}^{\gamma\gamma'}\left\langle c_{\mathbf{k}'\gamma}^{\dagger}c_{-\mathbf{k}'\gamma'}^{\dagger}\right\rangle\left\langle c_{-\mathbf{k}\gamma'}c_{\mathbf{k}\gamma}\right\rangle=\sum_{\mathbf{k}}\Delta_{\mathbf{k}}^{\gamma\gamma'}\left\langle c_{\mathbf{k}\gamma}^{\dagger}c_{-\mathbf{k}\gamma'}^{\dagger}\right\rangle. \tag{D.18}$$

Projected to a single superconducting channel, the Hamiltonian is

$$\begin{aligned}P_{\gamma\gamma'}^{-}\left(H^{0}+H^{V}-\mu N\right)=\varepsilon_{\gamma\gamma'}&+\sum_{\mathbf{k}}\left(\xi_{\mathbf{k}}c_{\mathbf{k}\gamma}^{\dagger}c_{\mathbf{k}\gamma}+\delta_{\gamma,-\gamma'}\xi_{\mathbf{k}}c_{\mathbf{k}\gamma'}^{\dagger}c_{\mathbf{k}\gamma'}\right)\\&-\sum_{\mathbf{k}}\left(\bar{\Delta}_{\mathbf{k}}^{\gamma\gamma'}c_{-\mathbf{k}\gamma'}c_{\mathbf{k}\gamma}+\Delta_{\mathbf{k}}^{\gamma\gamma'}c_{\mathbf{k}\gamma}^{\dagger}c_{-\mathbf{k}\gamma'}^{\dagger}\right).\end{aligned} \tag{D.19}$$

Channel solutions

An interaction for a given channel may be written as

$$v_{\mathbf{k}\mathbf{k}'}=\bar{v}_{\mathbf{k}'\mathbf{k}}=-v_{0}\bar{f}_{\mathbf{k}}\cdot g_{\mathbf{k}'}, \tag{D.20}$$

where we suppress the channel and band indexes here and in the following when there is no ambiguity. The channels are further split according to angular momentum, and the individual channels and their weights are summarized below. The order parameter is

$$\chi_{0}=v_{0}\sum_{\mathbf{k}}\bar{g}_{\mathbf{k}}\left\langle c_{-\mathbf{k}\gamma'}c_{\mathbf{k}\gamma}\right\rangle, \tag{D.21}$$

thus $\Delta_{\mathbf{k}}=f_{\mathbf{k}}\cdot\chi_{0}$. Note that we allow $f_{\mathbf{k}}$, $g_{\mathbf{k}}$, and χ_{0} to be either scalar or vector quantities.

The Hamiltonian in equation (D.19) is again identical in structure to the BCS Hamiltonian, however the parameter $\Delta_{\mathbf{k}}$ must be allowed complex as multiple channels may differ by relative phases which cannot be removed by a global unitary transformation. The solutions for each channel all share an identical form; however, for the intravalley channels, the expression for the eigenvalues $\lambda_{\mathbf{k}}$ and other associated expressions is modified according to $\xi \to \xi/2$, since the kinetic energy is split between each valley. To keep track of the two cases, we will write ξ', where $\xi' = \xi$ for intervalley channels and $\xi' = \xi/2$ for intravalley channels.

The diagonalized form is

$$P\left(H^0 + H^V - \mu N\right) = \sum_{\mathbf{k}} \sum_{\alpha=\gamma,\gamma'} \lambda_{\mathbf{k}} b^\dagger_{\mathbf{k}\alpha} b_{\mathbf{k}\alpha} + \sum_{\mathbf{k}} \left(\xi'_{\mathbf{k}} - \lambda_{\mathbf{k}}\right) + \varepsilon, \tag{D.22}$$

with eigenvalues

$$\lambda_{\mathbf{k}} = \sqrt{\xi'^2_{\mathbf{k}} + |\Delta_{\mathbf{k}}|^2}. \tag{D.23}$$

The Bogoliubov transformation for complex $\Delta_{\mathbf{k}}$ is

$$c_{\mathbf{k}\gamma} = e^{-i\delta_{\mathbf{k}}} \cos\beta_{\mathbf{k}} b_{\mathbf{k}\gamma} + e^{i\delta'_{\mathbf{k}}} \sin\beta_{\mathbf{k}} b^\dagger_{-\mathbf{k}\gamma'}, \tag{D.24a}$$

$$c_{-\mathbf{k}\gamma'} = e^{i\delta'_{\mathbf{k}}} \sin\beta_{\mathbf{k}} b^\dagger_{\mathbf{k}\gamma} - e^{-i\delta_{\mathbf{k}}} \cos\beta_{\mathbf{k}} b_{-\mathbf{k}\gamma'}, \tag{D.24b}$$

where $\delta'_{\mathbf{k}} - \delta_{\mathbf{k}} = \arg\Delta_{\mathbf{k}}$ and

$$\sin 2\beta_{\mathbf{k}} = -|\Delta_{\mathbf{k}}|/\lambda_{\mathbf{k}}, \tag{D.25a}$$

$$\cos 2\beta_{\mathbf{k}} = \quad \xi'_{\mathbf{k}}/\lambda_{\mathbf{k}}. \tag{D.25b}$$

Note also the inverse,

$$b_{\mathbf{k}\gamma} = e^{i\delta_{\mathbf{k}}} \cos\beta_{\mathbf{k}} c_{\mathbf{k}\gamma} + e^{i\delta'_{\mathbf{k}}} \sin\beta_{\mathbf{k}} c^\dagger_{-\mathbf{k}\gamma'}, \tag{D.26a}$$

$$b_{-\mathbf{k}\gamma'} = e^{i\delta'_{\mathbf{k}}} \sin\beta_{\mathbf{k}} c^\dagger_{\mathbf{k}\gamma} - e^{i\delta_{\mathbf{k}}} \cos\beta_{\mathbf{k}} c_{-\mathbf{k}\gamma'}. \tag{D.26b}$$

With this, Equation (D.21) becomes

$$\begin{aligned}\chi_0 &= v_0 \sum_{\mathbf{k}} \bar{g}_{\mathbf{k}} \left(-\frac{1}{2} e^{i \arg \Delta_{\mathbf{k}}} \sin 2\beta_{\mathbf{k}} \right), \\ &= \frac{v_0}{2} \sum_{\mathbf{k}} \bar{g}_{\mathbf{k}} \frac{|\Delta_{\mathbf{k}}| e^{i \arg \Delta_{\mathbf{k}}}}{\lambda_{\mathbf{k}}}, \\ &= \frac{v_0}{2} \sum_{\mathbf{k}} \bar{g}_{\mathbf{k}} \frac{\Delta_{\mathbf{k}}}{\lambda_{\mathbf{k}}}, \\ &= \frac{v_0}{2} \sum_{\mathbf{k}} \bar{g}_{\mathbf{k}} \frac{f_{\mathbf{k}} \cdot \chi_0}{\lambda_{\mathbf{k}}}.\end{aligned} \tag{D.27}$$

Gap equation

We now derive the gap equation for each symmetry channel. These are reduced to an integral which may be solved numerically.

Scalar channels

For scalar channels, $f_{\mathbf{k}} = g_{\mathbf{k}}$. We replace the sum by an integral, and since $|f_{\mathbf{k}}|^2$ and $\lambda_{\mathbf{k}}$ depend only on $|\mathbf{k}|$, the integral over ϕ is trivial and yields a factor of 2π. Equation (D.27) becomes

$$1 = \pi v_0 \int_{-\omega}^{\omega} \frac{|f(\xi)|^2 |\rho(\xi)| \, \mathrm{d}\xi}{\sqrt{\xi'^2 + |f(\xi)|^2 |\chi_0|^2}}, \tag{D.28}$$

where $\omega < \lambda$ is the energy cutoff around the chemical potential and the density of states is

$$\rho(\xi) = k \frac{\partial k}{\partial \xi} = \frac{2(\xi + \mu) - \lambda}{(at)^2}. \tag{D.29}$$

Vector channels

For the intervalley vector channels,

$$f_{\mathbf{k}} = g_{\mathbf{k}} = \sqrt{2}\sin\theta_{\mathbf{k}}\hat{\mathbf{k}}, \tag{D.30a}$$

$$\chi_0 = \left(|\chi_0|/\sqrt{2}\right)(\hat{e}_1 + i\hat{e}_2), \tag{D.30b}$$

for some fixed unit vectors $\hat{e}_1$ and $\hat{e}_2$. We consider two cases: $\hat{e}_1 \parallel \hat{e}_2$ or $\hat{e}_1 \perp \hat{e}_2$.

When $\hat{e}_1 \parallel \hat{e}_2$, write $\chi_0 = |\chi_0|\hat{e}e^{i\phi_0}$ and $\hat{\mathbf{k}}\cdot\hat{e} = \cos(\phi_{\mathbf{k}} - \phi_e)$, so equation (D.27) reads

$$\hat{e} = \frac{v_0}{2}\sum_{\mathbf{k}} \frac{|f_{\mathbf{k}}|^2}{\lambda_{\mathbf{k}}}\left(\hat{e}\cdot\hat{\mathbf{k}}\right)\hat{\mathbf{k}}. \tag{D.31}$$

Dotting both sides with $\hat{e}$ and converting to integral form,

$$1 = \frac{v_0}{2}\int_{-\omega}^{\omega}\int_0^{2\pi} \frac{|f(\xi)|^2\cos^2\phi|\rho(\xi)|\,\mathrm{d}\phi\,\mathrm{d}\xi}{\sqrt{\xi^2 + |f(\xi)|^2|\chi_0|^2\cos^2\phi}}, \tag{D.32}$$

where as expected by symmetry, the integral has been made independent of the direction of $\hat{e}$ through the substitution $\phi \to \phi + \phi_e$. The integral over ϕ can be written in terms of elliptical functions using the identity

$$\begin{aligned}\frac{a^2}{2}\int_0^{2\pi}\frac{\cos^2\phi\,\mathrm{d}\phi}{\sqrt{1+a^2\cos^2\phi}} &= E(-a^2) - K(-a^2) \\ &\quad + \sqrt{1+a^2}E\left(\frac{a^2}{1+a^2}\right) - \frac{1}{\sqrt{1+a^2}}K\left(\frac{a^2}{1+a^2}\right).\end{aligned} \tag{D.33}$$

When $\hat{e}_1 \perp \hat{e}_2$, then we may write $\hat{e}_1\cdot\hat{\mathbf{k}} = \cos(\phi_{\mathbf{k}} - \phi_1)$ and $\hat{e}_2\cdot\hat{\mathbf{k}} = \sin(\phi_{\mathbf{k}} - \phi_1)$, thus

$$\hat{e}_1 + i\hat{e}_2 = \frac{v_0}{2}\sum_{\mathbf{k}}\frac{|f_{\mathbf{k}}|^2}{\lambda_{\mathbf{k}}}\left[(\hat{e}_1 + i\hat{e}_2)\cdot\hat{\mathbf{k}}\right]\hat{\mathbf{k}}, \tag{D.34}$$

and dotting both sides by $\hat{e}_1 - i\hat{e}_2$ gives

$$2 = \frac{v_0}{2}\sum_{\mathbf{k}}\frac{|f_{\mathbf{k}}|^2}{\sqrt{\xi_{\mathbf{k}}^2 + (1/2)|f_{\mathbf{k}}|^2|\chi_0|^2}}. \tag{D.35}$$

Converting to integral form,

$$1 = \frac{\pi v_0}{2} \int_{-\omega}^{\omega} \frac{|f(\xi)|^2 |\rho(\xi)| \, \mathrm{d}\xi}{\sqrt{\xi^2 + (1/2)|f(\xi)|^2 |\chi_0|^2}}. \tag{D.36}$$

D.3 Spin expectation values

The full ground state in the superconducting system is

$$\prod_{\mathbf{k}} c^{\dagger}_{\mathbf{k}\bar{\uparrow}} c^{\dagger}_{\mathbf{k}\bar{\downarrow}} |\Omega\rangle , \tag{D.37}$$

where the bar notation denotes states in the lower valance band, i.e., if $\alpha = (\tau, \sigma)$ then $\bar{\alpha} = (-\tau, \sigma)$. The total spin operator is

$$\mathbf{S} = \sum_{\mathbf{k}} \mathbf{s}(\mathbf{k}) = \frac{1}{2} \sum_{\mathbf{k}} [\mathbf{s}(\mathbf{k}) + \mathbf{s}(-\mathbf{k})] , \tag{D.38}$$

where

$$\mathbf{s}(\mathbf{k}) = \frac{1}{2} \sum_{\substack{n,\tau \\ \sigma,\sigma'}} \boldsymbol{\sigma}_{\sigma\sigma'} {c^n_{\tau\sigma}}^{\dagger}(\mathbf{k}) \, c^n_{\tau\sigma'}(\mathbf{k}) \tag{D.39}$$

is the spin operator for a given $\mathbf{k}$, with $\boldsymbol{\sigma}_{\sigma\sigma'} = (\sigma^x_{\sigma\sigma'}, \sigma^y_{\sigma\sigma'}, \sigma^z_{\sigma\sigma'})$.

We wish to compute $\langle \mathbf{S} \rangle$ and $\langle \mathbf{S}^2 \rangle$ in the intervalley pairing state. The former follows from the value of $\langle \mathbf{s}(\mathbf{k}) \rangle$, and the latter from the spin of Cooper pairs, $\left\langle [\mathbf{s}(\mathbf{k}) + \mathbf{s}(-\mathbf{k})]^2 \right\rangle$. To see this, note that only cross terms with the same or opposite $\mathbf{k}$ contribute, so that

$$\langle \mathbf{S}^2 \rangle = \frac{1}{2} \sum_{\mathbf{k}} \left\langle [\mathbf{s}(\mathbf{k}) + \mathbf{s}(-\mathbf{k})]^2 \right\rangle . \tag{D.40}$$

Thus, we must compute $\langle \mathbf{s}(\mathbf{k}) \rangle$, $\left\langle [\mathbf{s}(\mathbf{k})]^2 \right\rangle$, and $\langle \mathbf{s}(\mathbf{k}) \cdot \mathbf{s}(-\mathbf{k}) \rangle$. In the remainder of this section, equality for the operator $\mathbf{s}(\mathbf{k})$ will denote equality of operators which have equivalent values on all three of these expectation values.

Only terms with $n = -1$ will contribute to the expectation value, thus we write

$$\mathbf{s}(\mathbf{k}) = \frac{1}{2}\sum_{\alpha} \boldsymbol{\sigma}_{\alpha\alpha} c^{\dagger}_{\mathbf{k}\alpha} c_{\mathbf{k}\alpha} + \boldsymbol{\sigma}_{\alpha\alpha} c^{\dagger}_{\mathbf{k}\bar{\alpha}} c_{\mathbf{k}\bar{\alpha}} + \boldsymbol{\sigma}_{\alpha,-\alpha} c^{\dagger}_{\mathbf{k}\alpha} c_{\mathbf{k},-\bar{\alpha}} + \boldsymbol{\sigma}_{\alpha,-\alpha} c^{\dagger}_{\mathbf{k}\bar{\alpha}} c_{\mathbf{k},-\alpha}, \quad \text{(D.41)}$$

and obtain

$$\langle \mathbf{s}(\mathbf{k}) \rangle = \frac{1}{2}\left(1 + \sin^2 \beta_{\mathbf{k}}\right) \operatorname{Tr} \boldsymbol{\sigma} = \mathbf{0}. \quad \text{(D.42)}$$

Next, we compute

$$\begin{aligned} \langle \mathbf{s}(\mathbf{k}) \cdot \mathbf{s}(\mathbf{k}') \rangle = {} & \frac{1}{4}\sum_{\alpha\alpha'} \boldsymbol{\sigma}_{\alpha\alpha} \cdot \boldsymbol{\sigma}_{\alpha'\alpha'} \left(1 + \sin^2 \beta_{\mathbf{k}} + \sin^2 \beta_{\mathbf{k}'}\right) \\ & + \frac{1}{4}\sum_{\alpha\alpha'} \boldsymbol{\sigma}_{\alpha\alpha} \cdot \boldsymbol{\sigma}_{\alpha'\alpha'} \left\langle c^{\dagger}_{\mathbf{k}\alpha} c_{\mathbf{k}\alpha} c^{\dagger}_{\mathbf{k}'\alpha'} c_{\mathbf{k}'\alpha'} \right\rangle \\ & + \frac{1}{4}\sum_{\alpha\alpha'} \boldsymbol{\sigma}_{\alpha,-\alpha} \cdot \boldsymbol{\sigma}_{\alpha',-\alpha'} \left\langle c^{\dagger}_{\mathbf{k}\bar{\alpha}} c_{\mathbf{k},-\alpha} c^{\dagger}_{\mathbf{k}'\alpha'} c_{\mathbf{k}',-\bar{\alpha}'} \right\rangle . \end{aligned} \quad \text{(D.43)}$$

The above expectation values are readily simplified using Wick's theorem,

$$\begin{aligned} \langle \mathbf{s}(\mathbf{k}) \cdot \mathbf{s}(\mathbf{k}') \rangle = {} & \frac{1}{4}\sum_{\alpha\alpha'} \boldsymbol{\sigma}_{\alpha\alpha} \cdot \boldsymbol{\sigma}_{\alpha'\alpha'} \frac{1}{4} \sin^2 2\beta_{\mathbf{k}} \left(\delta_{\mathbf{k},\mathbf{k}'}\delta_{\alpha,\alpha'} + \delta_{\mathbf{k},-\mathbf{k}'}\delta_{\alpha,-\alpha'}\right) \\ & + \frac{1}{4}\sum_{\alpha} \boldsymbol{\sigma}_{\alpha,-\alpha} \cdot \boldsymbol{\sigma}_{-\alpha,\alpha} \delta_{\mathbf{k},\mathbf{k}'} \cos^2 \beta_{\mathbf{k}}. \end{aligned} \quad \text{(D.44)}$$

Evaluating the sum gives,

$$\langle \mathbf{s}(\mathbf{k}) \cdot \mathbf{s}(\mathbf{k}') \rangle = \frac{1}{8} \sin^2 2\beta_{\mathbf{k}} \left(\delta_{\mathbf{k},\mathbf{k}'} - \delta_{\mathbf{k},-\mathbf{k}'}\right) + \delta_{\mathbf{k},\mathbf{k}'} \cos^2 \beta_{\mathbf{k}}, \quad \text{(D.45)}$$

which shows

$$\left\langle [\mathbf{s}(\mathbf{k}) + \mathbf{s}(-\mathbf{k})]^2 \right\rangle = 2\langle \mathbf{s}(\mathbf{k}) \cdot \mathbf{s}(-\mathbf{k}) \rangle + 2\left\langle \mathbf{s}(\mathbf{k})^2 \right\rangle, \quad \text{(D.46a)}$$

$$= 2\cos^2 \beta_{\mathbf{k}} - \frac{\delta_{\mathbf{k},\mathbf{0}}}{4} \sin^2 2\beta_{\mathbf{k}}. \quad \text{(D.46b)}$$

Far from the chemical potential (where $\mathbf{k} = 0$), $\sin^2 2\beta_{\mathbf{k}}$ approaches zero while $\cos^2 \beta_{\mathbf{k}}$ approaches unity. Thus, we neglect the second term above and obtain

$$\langle \mathbf{S}^2 \rangle = \sum_{\mathbf{k}} \cos^2 \beta_{\mathbf{k}}. \quad \text{(D.47)}$$

D.4 Berry curvature

Normal states

In the non-interacting system, the band resolved Berry curvature is

$$\mathbf{\Omega}^{n}_{\tau\sigma}\left(\mathbf{k}\right) = i\nabla_{\mathbf{k}} \times \left\langle u^{n}_{\tau\sigma}\left(\mathbf{k}\right) \left| \nabla_{\mathbf{k}} \right| u^{n}_{\tau\sigma}\left(\mathbf{k}\right)\right\rangle . \tag{D.48}$$

This can be computed directly by first considering

$$\begin{aligned}\left\langle u^{n}_{\tau\sigma}\left(\mathbf{k}\right) \left| \nabla_{\mathbf{k}} \right| u^{n}_{\tau\sigma}\left(\mathbf{k}\right)\right\rangle = &\sum_{\nu} \bar{M}^{\nu n}_{\tau\sigma}\left(\mathbf{k}\right) \nabla_{\mathbf{k}} M^{\nu n}_{\tau\sigma}\left(\mathbf{k}\right) \\ &+ \sum_{\nu,\nu'} \bar{M}^{\nu n}_{\tau\sigma}\left(\mathbf{k}\right) M^{\nu' n}_{\tau\sigma}\left(\mathbf{k}\right) \left\langle v^{\nu}_{\tau\sigma}\left(\mathbf{k}\right) \middle| \nabla_{\mathbf{k}} \middle| v^{\nu'}_{\tau\sigma}\left(\mathbf{k}\right)\right\rangle .\end{aligned} \tag{D.49}$$

The second term is effectively zero by an argument similar to the one given below in section E.1. Using the identities

$$\frac{\partial}{\partial k} M^{\nu n}_{\tau\sigma}\left(\mathbf{k}\right) = n\tau \frac{\partial}{\partial k} \theta^{n}_{\tau\sigma}\left(k\right), \tag{D.50a}$$

$$\frac{\partial}{\partial \phi} M^{\nu n}_{\tau\sigma}\left(\mathbf{k}\right) = i\tau M^{\nu n}_{\tau\sigma}\left(\mathbf{k}\right) \delta_{\nu,-1}, \tag{D.50b}$$

gives the z-component of the curvature,

$$\Omega^{n}_{\tau\sigma}\left(k\right) = \hat{\mathbf{z}} \cdot \mathbf{\Omega}^{n}_{\tau\sigma}\left(\mathbf{k}\right) \tag{D.51a}$$

$$= -n\tau \left[\frac{1}{2k} \frac{\partial}{\partial k} \theta^{n}_{\tau\sigma}\left(k\right)\right] \sin \theta^{n}_{\tau\sigma}\left(k\right), \tag{D.51b}$$

$$= -n\tau \frac{2(at)^2(\Delta - \lambda\tau\sigma)}{\left[\left(2atk\right)^2 + \left(\Delta - \lambda\tau\sigma\right)^2\right]^{3/2}}. \tag{D.51c}$$

The Berry curvature of left and right circularly polarized ($\boldsymbol{\epsilon}_{\pm}$) optical excitations for a given $\mathbf{k}$ then follows to be $\pm 2\Omega^{+}_{+\uparrow}\left(k\right)$.

BCS States

We again consider the intervalley pairing state. The BCS ground state is[2]

$$|\Omega\rangle = \prod_{\mathbf{k}} \csc\beta_{\mathbf{k}} b_{\mathbf{k}\uparrow} b_{-\mathbf{k}\downarrow} |0\rangle\,, \tag{D.52a}$$

$$= \prod_{\mathbf{k}} \left(\cos\beta_{\mathbf{k}} - \sin\beta_{\mathbf{k}} c^{\dagger}_{\mathbf{k}\uparrow} c^{\dagger}_{-\mathbf{k}\downarrow}\right) |0\rangle\,. \tag{D.52b}$$

This may be viewed as built up from the single-quasiparticle eigenstates,

$$|\mathbf{k}\rangle = \csc\beta_{\mathbf{k}} b_{\mathbf{k}\uparrow} b_{-\mathbf{k}\downarrow} |0\rangle\,, \tag{D.53}$$

of the $\mathbf{k}$ dependent Hamiltonian $\lambda_{\mathbf{k}} b^{\dagger}_{\mathbf{k}\uparrow} b_{\mathbf{k}\uparrow} - \lambda_{\mathbf{k}} b_{-\mathbf{k}\downarrow} b^{\dagger}_{-\mathbf{k}\downarrow}$. Thus, consider the z-component of the Berry curvature of this state,

$$\Omega_{\mathbf{k}} = \hat{\mathbf{z}} \cdot i\nabla_{\mathbf{k}} \times \langle \mathbf{k} \,|\, \nabla_{\mathbf{k}} \,|\, \mathbf{k}\rangle\,, \tag{D.54a}$$

$$= \hat{\mathbf{z}} \cdot i\nabla_{\mathbf{k}} \times \left\langle 0 \,\middle|\, c_{-\mathbf{k}\downarrow} c_{\mathbf{k}\uparrow} \nabla_{\mathbf{k}} \left(c^{\dagger}_{\mathbf{k}\uparrow} c^{\dagger}_{-\mathbf{k}\downarrow}\right) \,\middle|\, 0\right\rangle, \tag{D.54b}$$

$$= \Omega^{-}_{+\uparrow}(k) + \Omega^{-}_{-\downarrow}(-k) = 0. \tag{D.54c}$$

To see why equation (D.54b) follows from equation (D.54a), write $|\mathbf{k}\rangle = \cos\beta_{\mathbf{k}} - \sin\beta_{\mathbf{k}} c^{\dagger}_{\mathbf{k}\uparrow} c^{\dagger}_{-\mathbf{k}\downarrow}$ and consider each of the resulting four cross terms: one contains no operators, will be proportional to $\mathbf{k}$, independent of $\phi_{\mathbf{k}}$, and thus have vanishing curl; the two terms with a pair of either creation or annihilation operators have zero expectation value; this leaves only the term given in equation (D.54b). Equation (D.54c) now follows since $|0\rangle$ is independent of $\mathbf{k}$ and the Berry curvature is additive over non-interacting states.

[2]Note that the full ground state also contains the lower two filled bands, but those contribute zero net Berry curvature and may be ignored.

Optical excitations

A single optically excited state in the left valley for a given $\mathbf{k}$ is

$$c_{+\uparrow}^{+\,\dagger}(\mathbf{k})\, c_{\mathbf{k}\uparrow}\,|\mathbf{k}\rangle\,, \tag{D.55a}$$

$$= c_{+\uparrow}^{+\,\dagger}(\mathbf{k})\left(\cos\beta_{\mathbf{k}} b_{\mathbf{k}\uparrow} + \sin\beta_{\mathbf{k}} b_{-\mathbf{k}\downarrow}^{\dagger}\right)|\mathbf{k}\rangle\,, \tag{D.55b}$$

$$= \sin\beta_{\mathbf{k}} c_{+\uparrow}^{+\,\dagger}(\mathbf{k})\, b_{-\mathbf{k}\downarrow}^{\dagger}\,|\mathbf{k}\rangle\,, \tag{D.55c}$$

$$= c_{+\uparrow}^{+\,\dagger}(\mathbf{k})\, b_{-\mathbf{k}\downarrow}^{\dagger} b_{\mathbf{k}\uparrow} b_{-\mathbf{k}\downarrow}\,|0\rangle\,, \tag{D.55d}$$

$$= -\sin^2\beta_{\mathbf{k}} c_{+\uparrow}^{+\,\dagger}(\mathbf{k})\, b_{\mathbf{k}\uparrow}\,|0\rangle\,, \tag{D.55e}$$

$$= -\sin^3\beta_{\mathbf{k}} c_{+\uparrow}^{+\,\dagger}(\mathbf{k})\, c_{-\downarrow}^{-\,\dagger}(-\mathbf{k})\,|0\rangle\,, \tag{D.55f}$$

which has corresponding Berry Curvature

$$\Omega_{\mathbf{k}}^{L} = \sin^6\beta_{\mathbf{k}}\left[\Omega_{+\uparrow}^{+}(k) + \Omega_{-\downarrow}^{-}(-k)\right], \tag{D.56a}$$

$$= 2\sin^6\beta_{\mathbf{k}}\Omega_{+\uparrow}^{+}(k)\,. \tag{D.56b}$$

A single optically excited state in the right valley for a given $\mathbf{k}$ is

$$c_{-\downarrow}^{+\,\dagger}(-\mathbf{k})\, c_{-\mathbf{k}\downarrow}\,|\mathbf{k}\rangle\,, \tag{D.57a}$$

$$= c_{-\downarrow}^{+\,\dagger}(\mathbf{k})\left(-\cos\beta_{\mathbf{k}} b_{-\mathbf{k}\downarrow} + \sin\beta_{\mathbf{k}} b_{\mathbf{k}\uparrow}^{\dagger}\right)|\mathbf{k}\rangle\,, \tag{D.57b}$$

$$= \sin\beta_{\mathbf{k}} c_{-\downarrow}^{+\,\dagger}(\mathbf{k})\, b_{\mathbf{k}\uparrow}^{\dagger}\,|\mathbf{k}\rangle\,, \tag{D.57c}$$

$$= c_{-\downarrow}^{+\,\dagger}(\mathbf{k})\, b_{\mathbf{k}\uparrow}^{\dagger} b_{\mathbf{k}\uparrow} b_{-\mathbf{k}\downarrow}\,|0\rangle\,, \tag{D.57d}$$

$$= \sin^2\beta_{\mathbf{k}} c_{-\downarrow}^{+\,\dagger}(\mathbf{k})\, b_{-\mathbf{k}\downarrow}\,|0\rangle\,, \tag{D.57e}$$

$$= \sin^3\beta_{\mathbf{k}} c_{-\downarrow}^{+\,\dagger}(\mathbf{k})\, c_{+\uparrow}^{-\,\dagger}(\mathbf{k})\,|0\rangle\,, \tag{D.57f}$$

which has corresponding Berry Curvature

$$\Omega_{\mathbf{k}}^{R} = \sin^{6}\beta_{\mathbf{k}}\left[\Omega_{-\downarrow}^{+}(k) + \Omega_{+\uparrow}^{-}(k)\right], \tag{D.58a}$$

$$= -2\sin^{6}\beta_{\mathbf{k}}\Omega_{+\uparrow}^{+}(k), \tag{D.58b}$$

$$= -\Omega_{\mathbf{k}}^{L}. \tag{D.58c}$$

Appendix E

Optical Transitions

E.1 Single electron transitions

Consider the spin-orbit Hamiltonian for a single non-interacting electron which includes a position dependent potential $W(\mathbf{Q})$ and an electromagnetic potential $\mathbf{A}(\mathbf{Q})$,

$$H = \frac{(\mathbf{P} + e\mathbf{A})^2}{2M} + \lambda \mathbf{L} \cdot \mathbf{S} + W. \tag{E.1}$$

Given $\mathbf{L} = \mathbf{Q} \times \mathbf{P}$, one can show, either via the commutation relations or formal differentiation, that the velocity operator is

$$\mathbf{V} = i\,[H, \mathbf{Q}] = \frac{\partial H}{\partial \mathbf{P}} = \frac{\mathbf{P} + e\mathbf{A}}{M} + \lambda \mathbf{Q} \times \mathbf{S}. \tag{E.2}$$

In a gauge with $\nabla \cdot \mathbf{A} = 0$,

$$H = \frac{\mathbf{P}^2}{2M} + \frac{e}{M}\mathbf{A} \cdot \mathbf{P} + e^2\mathbf{A}^2. \tag{E.3}$$

For monochromatic optical perturbations with amplitude A_0, wave vector $\mathbf{q}$, frequency ω, and polarization vector $\boldsymbol{\epsilon}$, the electromagnetic potential is of the form

$$\mathbf{A} = 2\,\mathrm{Re}\,\boldsymbol{\epsilon} A_0 e^{i(\mathbf{q}\cdot\mathbf{Q} - \omega t)}. \tag{E.4}$$

For linear perturbations, we neglect the term of order $\mathbf{A}^2$ to write the Hamiltonian in the form

$$H = H_0 + H' e^{-i\omega t} + H'^{\dagger} e^{i\omega t}. \tag{E.5}$$

Here, $H' = eA_0 e^{i\mathbf{q}\cdot\mathbf{Q}} (\boldsymbol{\epsilon} \cdot \mathbf{V})$ appears as a standard harmonic perturbation where $\mathbf{V} = i[H_0, \mathbf{Q}]$ is the velocity operator for the unperturbed system. Thus, according to Fermi's golden rule, the optical transition probability per unit time is

$$\Gamma_{f \leftarrow i} = 2\pi e^2 A_0^2 \left| \langle f \,|\, e^{i\mathbf{q}\cdot\mathbf{Q}} \boldsymbol{\epsilon} \cdot \mathbf{V} \,|\, i \rangle \right|^2 \delta \left(E_f + E_i - \omega \right). \tag{E.6}$$

Typically, the dipole approximation is used in which $e^{i\mathbf{q}\cdot\mathbf{Q}} \to 1$.

Tight-binding d-orbital transitions

In a noninteracting system of Bloch electrons, $\nabla_{\mathbf{k}} H_{\mathbf{k}} = \mathbf{V}_{\mathbf{k}}$. Thus, for each $\mathbf{k}$, the matrix element appearing in the optical transition rate (in the dipole approximation) may be computed as

$$\langle \psi_{n'\mathbf{k}} \,|\, \mathbf{V} \,|\, \psi_{n\mathbf{k}} \rangle = \langle u_{n'\mathbf{k}} \,|\, \mathbf{V}_{\mathbf{k}} \,|\, u_{n\mathbf{k}} \rangle = \langle u_{n'\mathbf{k}} \,|\, \nabla_{\mathbf{k}} H_{\mathbf{k}} \,|\, u_{n\mathbf{k}} \rangle . \tag{E.7}$$

The matrix elements of the derivative, $\langle u_{n\mathbf{k}} \,|\, \nabla_{\mathbf{k}} H_{\mathbf{k}} \,|\, u_{n'\mathbf{k}} \rangle$, appearing in the optical translation rate may be cumbersome to compute. We show that in the tight-binding approximation with only d-type orbitals, it is sufficient to compute the derivative of the orbital matrix elements, $\nabla_{\mathbf{k}} H_{\mathbf{k}}^{\nu\nu'} = \nabla_{\mathbf{k}} \langle v_{\nu\mathbf{k}} \,|\, H_{\mathbf{k}} \,|\, v_{\nu'\mathbf{k}} \rangle$.

We have

$$H_{\mathbf{k}} = \sum_{n\mathbf{k}'} E_{n\mathbf{k}'} T_{\mathbf{k}} \,|\psi_{n\mathbf{k}'}\rangle \langle \psi_{n\mathbf{k}'}|\, T_{\mathbf{k}}^{-1} = H_{\mathbf{k}}^0 + H_{\mathbf{k}}^1, \tag{E.8}$$

where

$$H^0_{\mathbf{k}} = \sum_{\nu,\nu'} H^{\nu\nu'}_{\mathbf{k}} \left|v_{\nu\mathbf{k}}\right\rangle \left\langle v_{\nu'\mathbf{k}}\right|, \tag{E.9a}$$

$$H^1_{\mathbf{k}} = \sum_{\nu,\nu'} \sum_{\mathbf{k}'\neq\mathbf{k}} H^{\nu\nu'}_{\mathbf{k}'} T_{\mathbf{k}-\mathbf{k}'} \left|v_{\nu\mathbf{k}'}\right\rangle \left\langle v_{\nu'\mathbf{k}'}\right| T^{-1}_{\mathbf{k}-\mathbf{k}'}. \tag{E.9b}$$

First, using $\nabla_{\mathbf{k}} H^1_{\mathbf{k}} = i\left[H^1_{\mathbf{k}}, \mathbf{Q}\right]$, we obtain a sum over $\mathbf{k}' \neq \mathbf{k}$ of terms proportional to $\delta_{\mathbf{k},\mathbf{k}'}$, thus all matrix elements for $\nabla_{\mathbf{k}} H^1_{\mathbf{k}}$ vanish. Next, we have

$$\nabla_{\mathbf{k}} H^0_{\mathbf{k}} = \sum_{\nu,\nu'} \nabla_{\mathbf{k}} H^{\nu\nu'}_{\mathbf{k}} \left|v_{\nu\mathbf{k}}\right\rangle \left\langle v_{\nu'\mathbf{k}}\right| \tag{E.10a}$$

$$+ \sum_{\nu,\nu'} H^{\nu\nu'}_{\mathbf{k}} \left(\nabla_{\mathbf{k}} \left|v_{\nu\mathbf{k}}\right\rangle\right) \left\langle v_{\nu'\mathbf{k}}\right| \tag{E.10b}$$

$$+ \sum_{\nu,\nu'} H^{\nu\nu'}_{\mathbf{k}} \left|v_{\nu\mathbf{k}}\right\rangle \left(\nabla_{\mathbf{k}} \left\langle v_{\nu'\mathbf{k}}\right|\right). \tag{E.10c}$$

Using

$$\nabla_{\mathbf{k}} \left|v_{\nu\mathbf{k}}\right\rangle = \frac{T_{\mathbf{k}}}{i\sqrt{N}} \sum_{n=1}^{N} e^{i\mathbf{k}\cdot\mathbf{R}^0_n} T\left(\mathbf{R}^0_n\right) \mathbf{Q} \left|\varphi_\nu\right\rangle, \tag{E.11}$$

we find the sum in equation (E.10b) contains terms proportional to the local optical matrix elements $\left\langle \varphi_{\nu'} \middle| T\left(\mathbf{R}^0_n\right) \mathbf{Q} \middle| \varphi_\nu \right\rangle$. For finite $\mathbf{R}^0_n$, these off-center integrals are small, and for $\mathbf{R}^0_n = 0$, optical transitions between d-orbitals are forbidden by symmetry. Similar logic applies to the sum in equation (E.10a), thus

$$\left\langle u_{n\mathbf{k}} \middle| \nabla_{\mathbf{k}} H_{\mathbf{k}} \middle| u_{n'\mathbf{k}} \right\rangle \backsimeq \sum_{\nu,\nu'} \bar{M}^{\nu n}_{\mathbf{k}} \left(\nabla_{\mathbf{k}} H^{\nu\nu'}_{\mathbf{k}}\right) M^{\nu' n'}_{\mathbf{k}}. \tag{E.12}$$

In the case where $H^{\nu\nu'}_{\mathbf{k}}$ is linear in $\mathbf{k}$, computing this derivative is equivalent to using minimal substitution, i.e., $H^{\nu\nu'}_{\mathbf{k}+e\mathbf{A}} = H^{\nu\nu'}_{\mathbf{k}} + eA\nabla_{\mathbf{k}} H^{\nu\nu'}_{\mathbf{k}}$.

E.2 Transitions in the TMD model

As remarked above, we may consider a perturbation of $H_{\tau\sigma}^{\nu\nu'}(\mathbf{k})$ arising from minimal coupling,

$$H_{\tau\sigma}^{\nu\nu'}(\mathbf{k}) \to H_{\tau\sigma}^{\nu\nu'}(\mathbf{k}+e\mathbf{A}) = H_{\tau\sigma}^{\nu\nu'}(\mathbf{k}) + h_{\tau}^{\nu\nu'}, \tag{E.13}$$

where in the dipole approximation, $\mathbf{A} = 2\,\mathrm{Re}\,\boldsymbol{\epsilon} A_0 e^{-i\omega t}$, $h_{\tau}^{vv} = h_{\tau}^{cc} = 0$, and

$$h_{\tau}^{vc} = \bar{h}_{\tau}^{cv} = 2ateA_0\,(\tau\hat{\mathbf{x}} + i\hat{\mathbf{y}}) \cdot \mathrm{Re}\,(\boldsymbol{\epsilon} e^{-i\omega t}). \tag{E.14}$$

Thus the optical perturbation operator is

$$H^A = \sum_{\mathbf{k}} \sum_{\tau,\sigma} h_{\tau}^{vc} a_{\tau\sigma}^{v\,\dagger}(\mathbf{k})\, a_{\tau\sigma}^{c}(\mathbf{k}) + \mathrm{h.c.} \tag{E.15}$$

Separating out the time dependence, we may write this in the standard form $H^A = H' e^{-i\omega t} + H'^{\dagger} e^{i\omega t}$, where

$$H' = \sum_{\mathbf{k}} \sum_{\tau,\sigma} H'_{\tau} a_{\tau\sigma}^{v\,\dagger}(\mathbf{k})\, a_{\tau\sigma}^{c}(\mathbf{k}) - \sum_{\mathbf{k}} \sum_{\tau,\sigma} H'_{-\tau} a_{\tau\sigma}^{c\,\dagger}(\mathbf{k})\, a_{\tau\sigma}^{v}(\mathbf{k}), \tag{E.16}$$

and

$$H'_{\tau} = ateA_0\,(\tau\hat{\mathbf{x}} + i\hat{\mathbf{y}}) \cdot \boldsymbol{\epsilon}. \tag{E.17}$$

Chancing basis, we recover the optical matrix element, $P_{\tau\sigma}^{nn'}(\mathbf{k}, \boldsymbol{\epsilon})$, now explicitly a function of the polarization vector,

$$H^A = \sum_{\mathbf{k}} \sum_{\tau,\sigma} \sum_{n,n'} \frac{eA_0}{m_0} P_{\tau\sigma}^{nn'}(\mathbf{k}, \boldsymbol{\epsilon})\, c_{\tau\sigma}^{n\,\dagger}(\mathbf{k})\, c_{\tau\sigma}^{n'}(\mathbf{k}). \tag{E.18}$$

For circularly polarized light, $\boldsymbol{\epsilon}_{\pm} = (\hat{\mathbf{x}} \pm i\hat{\mathbf{y}})/\sqrt{2}$ and

$$P_{\tau\sigma}^{+-}(\mathbf{k}, \boldsymbol{\epsilon}_{\pm}) = \mp\tau\sqrt{2}atm_0 e^{\pm i\phi} \sin^2 \frac{\theta_{\tau\sigma}^{\mp\tau}(k)}{2}. \tag{E.19}$$

A brief note about the units of P above. To conveniently express P in units of energy, multiply by $c/\hbar$. Typically, at is given in Å eV, the electron mass is given in

units of MeV/c^2, $\hbar$ in eV s, and c in Å s^{-1}. Thus when written as $(c/\hbar)P = pE_P$, where p is a unitless function of the energy, the important overall energy scale is $E_P = atm_0/(c\hbar) \times 10^3$GeV, where the symbols in E_P are the numerical magnitudes of the quantities when expressed in the assumed units above. In particular, $E_P = at \cdot 0.259\,\mathrm{GeV}$, and for $at = 3.2$, $E_P = 0.83\,\mathrm{GeV}$. Alternatively, one may write this in terms of fundamental constants: using $at = 3.2$ again gives $P = (1.624 \times 10^3 c\hbar m_0)\, p$.

Bibliography

[1]E. Sosenko, H. Wei, and V. Aji, "Effect of contacts on spin lifetime measurements in graphene", Phys. Rev. B **89**, 245436 (2014).

[2]J. Z. Evan Sosenko, and V. Aji, "Superconductivity in transition metal dichalcogenides", (2015).

[3]J. D. Hunter, "Matplotlib: a 2d graphics environment", Computing In Science & Engineering **9**, 90–95 (2007).

[4]K. S. Novoselov, A. K. Geim, S. V. Morozov, D. Jiang, Y. Zhang, S. V. Dubonos, I. V. Grigorieva, and A. A. Firsov, "Electric Field Effect in Atomically Thin Carbon Films", Science **306**, 666–669 (2004).

[5]G. Binasch, P. Grünberg, F. Saurenbach, and W. Zinn, "Enhanced magnetoresistance in layered magnetic structures with antiferromagnetic interlayer exchange", Phys. Rev. B **39**, 4828–4830 (1989).

[6]S. A. Wolf, D. D. Awschalom, R. A. Buhrman, J. M. Daughton, S. von Molnár, M. L. Roukes, A. Y. Chtchelkanova, and D. M. Treger, "Spintronics: a spin-based electronics vision for the future", Science **294**, 1488–1495 (2001).

[7]I. Žutić, J. Fabian, and S. Das Sarma, "Spintronics: fundamentals and applications", Rev. Mod. Phys. **76**, 323–410 (2004).

[8]S. Datta, and B. Das, "Electronic analog of the electro-optic modulator", Applied Physics Letters **56**, 665–667 (1990).

[9]F. J. Jedema, A. T. Filip, and B. J. van Wees, "Electrical spin injection and accumulation at room temperature in an all-metal mesoscopic spin valve", Nature **410**, 345–348 (2001).

[10]M. Johnson, and R. H. Silsbee, "Interfacial charge-spin coupling: injection and detection of spin magnetization in metals", Phys. Rev. Lett. **55**, 1790–1793 (1985).

[11]T. Yang, T. Kimura, and Y. Otani, "Giant spin-accumulation signal and pure spin-current-induced reversible magnetization switching", Nat Phys **4**, 851–854 (2008).

[12]S. O. Valenzuela, D. J. Monsma, C. M. Marcus, V. Narayanamurti, and M. Tinkham, "Spin polarized tunneling at finite bias", Phys. Rev. Lett. **94**, 196601 (2005).

[13]K. S. Novoselov, A. K. Geim, S. V. Morozov, D. Jiang, Y. Zhang, S. V. Dubonos, I. V. Grigorieva, and A. A. Firsov, "Electric field effect in atomically thin carbon films", Science **306**, 666–669 (2004).

[14]D. Huertas-Hernando, F. Guinea, and A. Brataas, "Spin-orbit coupling in curved graphene, fullerenes, nanotubes, and nanotube caps", Phys. Rev. B **74**, 155426 (2006).

[15]B. Trauzettel, D. V. Bulaev, D. Loss, and G. Burkard, "Spin qubits in graphene quantum dots", Nat Phys **3**, 192–196 (2007).

[16]N. Tombros, C. Jozsa, M. Popinciuc, H. T. Jonkman, and B. J. van Wees, "Electronic spin transport and spin precession in single graphene layers at room temperature", Nature **448**, 571–574 (2007).

[17]M. Ohishi, M. Shiraishi, R. Nouchi, T. Nozaki, T. Shinjo, and Y. Suzuki, "Spin injection into a graphene thin film at room temperature", Japanese Journal of Applied Physics **46**, L605–L607 (2007).

[18]S. Cho, Y.-F. Chen, and M. S. Fuhrer, "Gate-tunable graphene spin valve", Applied Physics Letters **91**, 123105 (2007) 10.1063/1.2784934.

[19]N. Tombros, S. Tanabe, A. Veligura, C. Jozsa, M. Popinciuc, H. T. Jonkman, and B. J. van Wees, "Anisotropic spin relaxation in graphene", Phys. Rev. Lett. **101**, 046601 (2008).

[20]E. Hill, A. Geim, K. Novoselov, F. Schedin, and P. Blake, "Graphene spin valve devices", Magnetics, IEEE Transactions on **42**, 2694–2696 (2006).

[21]W. Han, J.-R. Chen, D. Wang, K. M. McCreary, H. Wen, A. G. Swartz, J. Shi, and R. K. Kawakami, "Spin Relaxation in Single-Layer Graphene with Tunable Mobility", Nano Letters **12**, 3443–3447 (2012).

[22]W. Han, K. McCreary, K. Pi, W. Wang, Y. Li, H. Wen, J. Chen, and R. Kawakami, "Spin transport and relaxation in graphene", Journal of Magnetism and Magnetic Materials **324**, 369–381 (2012).

[23]C. Józsa, T. Maassen, M. Popinciuc, P. J. Zomer, A. Veligura, H. T. Jonkman, and B. J. van Wees, "Linear scaling between momentum and spin scattering in graphene", Phys. Rev. B **80**, 241403 (2009).

[24]M. Popinciuc, C. Józsa, P. J. Zomer, N. Tombros, A. Veligura, H. T. Jonkman, and B. J. van Wees, "Electronic spin transport in graphene field-effect transistors", Phys. Rev. B **80**, 214427 (2009).

[25]K. Pi, W. Han, K. M. McCreary, A. G. Swartz, Y. Li, and R. K. Kawakami, "Manipulation of spin transport in graphene by surface chemical doping", Phys. Rev. Lett. **104**, 187201 (2010).

[26]R. J. Elliott, "Theory of the effect of spin-orbit coupling on magnetic resonance in some semiconductors", Phys. Rev. **96**, 266–279 (1954).

[27]W. Han, and R. K. Kawakami, "Spin relaxation in single-layer and bilayer graphene", Phys. Rev. Lett. **107**, 047207 (2011).

[28]S. Takahashi, and S. Maekawa, "Spin injection and detection in magnetic nanostructures", Phys. Rev. B **67**, 052409 (2003).

[29]M. Wojtaszek, I. J. Vera-Marun, and B. J. van Wees, "Transition between 1D and 0D spin transport studied by Hanle precession", (2014).

[30]W. Han, K. Pi, K. M. McCreary, Y. Li, J. J. I. Wong, A. G. Swartz, and R. K. Kawakami, "Tunneling Spin Injection into Single Layer Graphene", Phys. Rev. Lett. **105**, 167202 (2010).

[31]M. Johnson, and R. H. Silsbee, "Coupling of electronic charge and spin at a ferromagnetic-paramagnetic metal interface", Phys. Rev. B **37**, 5312–5325 (1988).

[32]A. G. Swartz, K. M. McCreary, W. Han, H. Wen, and R. K. Kawakami, *A systematic approach to interpreting hanle spin precession data in non-local spin valves*, 2013.

[33]T. Maassen, I. J. Vera-Marun, M. H. D. Guimarães, and B. J. van Wees, "Contact-induced spin relaxation in Hanle spin precession measurements", Phys. Rev. B **86**, 235408 (2012).

[34]F. D. M. Haldane, "Model for a Quantum Hall Effect without Landau Levels: Condensed-Matter Realization of the "Parity Anomaly"", Phys. Rev. Lett. **61**, 2015–2018 (1988).

[35]C. L. Kane, and E. J. Mele, "Quantum Spin Hall Effect in Graphene", Phys. Rev. Lett. **95**, 226801 (2005).

[36]B. A. Bernevig, and S.-C. Zhang, "Quantum Spin Hall Effect", Phys. Rev. Lett. **96**, 106802 (2006).

[37]M. König, S. Wiedmann, C. Brüne, A. Roth, H. Buhmann, L. W. Molenkamp, X.-L. Qi, and S.-C. Zhang, "Quantum Spin Hall Insulator State in HgTe Quantum Wells", Science **318**, 766–770 (2007).

[38]M. Z. Hasan, and C. L. Kane, "*COLLOQUIUM*: TOPOLOGICAL INSULATORS", Rev. Mod. Phys. **82**, 3045–3067 (2010).

[39]X.-L. Qi, and S.-C. Zhang, "Topological insulators and superconductors", Rev. Mod. Phys. **83**, 1057–1110 (2011).

[40]W. Witczak-Krempa, G. Chen, Y. B. Kim, and L. Balents, "Correlated Quantum Phenomena in the Strong Spin-Orbit Regime", Annual Review of Condensed Matter Physics **5**, 57–82 (2014).

[41]B. Radisavljevic, A. Radenovic, J. Brivio, V. Giacometti, and A. Kis, "Single-layer MoS_2 transistors", Nat Nano **6**, 147–150 (2011).

[42]Z. Y. Zhu, Y. C. Cheng, and U. Schwingenschlögl, "Giant spin-orbit-induced spin splitting in two-dimensional transition-metal dichalcogenide semiconductors", Phys. Rev. B **84**, 153402 (2011).

[43]Y. Zhang, J. Ye, Y. Matsuhashi, and Y. Iwasa, "Ambipolar MoS_2 Thin Flake Transistors", Nano Letters **12**, PMID: 22276648, 1136–1140 (2012).

[44]Q. H. Wang, K. Kalantar-Zadeh, A. Kis, J. N. Coleman, and M. S. Strano, "Electronics and optoelectronics of two-dimensional transition metal dichalcogenides", Nat Nano **7**, 699–712 (2012).

[45]J. T. Ye, Y. J. Zhang, R. Akashi, M. S. Bahramy, R. Arita, and Y. Iwasa, "Superconducting Dome in a Gate-Tuned Band Insulator", Science **338**, 1193–1196 (2012).

[46]W. Bao, X. Cai, D. Kim, K. Sridhara, and M. S. Fuhrer, "High mobility ambipolar MoS_2 field-effect transistors: Substrate and dielectric effects", Applied Physics Letters **102**, 042104 (2013) 10.1063/1.4789365.

[47]F. Zahid, L. Liu, Y. Zhu, J. Wang, and H. Guo, "A generic tight-binding model for monolayer, bilayer and bulk MoS_2", AIP Advances **3**, 052111 (2013) 10.1063/1.4804936.

[48]E. Cappelluti, R. Roldán, J. A. Silva-Guillén, P. Ordejón, and F. Guinea, "Tight-binding model and direct-gap/indirect-gap transition in single-layer and multilayer MoS_2", Phys. Rev. B **88**, 075409 (2013).

[49]X. Xu, W. Yao, D. Xiao, and T. F. Heinz, "Spin and pseudospins in layered transition metal dichalcogenides", Nat Phys **10**, Review, 343–350 (2014).

[50]T. Das, and K. Dolui, "Superconducting dome in MoS_2 and $TiSe_2$ generated by quasiparticle-phonon coupling", Phys. Rev. B **91**, 094510 (2015).

[51]J. Lee, K. F. Mak, and J. Shan, "Electrical control of the valley Hall effect in bilayer MoS_2 transistors", (2015).

[52]R. A. Bromley, R. B. Murray, and A. D. Yoffe, "The band structures of some transition metal dichalcogenides. III. Group VIA: trigonal prism materials", Journal of Physics C: Solid State Physics **5**, 759 (1972).

[53]T. Böker, R. Severin, A. Müller, C. Janowitz, R. Manzke, D. Voß, P. Krüger, A. Mazur, and J. Pollmann, "Band structure of MoS_2, $MoSe_2$, and $\alpha - MoTe_2$ Angle-resolved photoelectron spectroscopy and *ab initio* calculations", Phys. Rev. B **64**, 235305 (2001).

[54]K. F. Mak, C. Lee, J. Hone, J. Shan, and T. F. Heinz, "Atomically Thin MoS_2: A New Direct-Gap Semiconductor", Phys. Rev. Lett. **105**, 136805 (2010).

[55]A. Splendiani, L. Sun, Y. Zhang, T. Li, J. Kim, C.-Y. Chim, G. Galli, and F. Wang, "Emerging Photoluminescence in Monolayer MoS_2", Nano Letters **10**, PMID: 20229981, 1271–1275 (2010).

[56]A. Kormányos, V. Zólyomi, N. D. Drummond, P. Rakyta, G. Burkard, and V. I. Fal'ko, "Monolayer MoS_2: Trigonal warping, the Γ valley, and spin-orbit coupling effects", Phys. Rev. B **88**, 045416 (2013).

[57]G.-B. Liu, W.-Y. Shan, Y. Yao, W. Yao, and D. Xiao, "Three-band tight-binding model for monolayers of group-VIB transition metal dichalcogenides", Phys. Rev. B **88**, 085433 (2013).

[58]D. Xiao, M.-C. Chang, and Q. Niu, "Berry phase effects on electronic properties", Rev. Mod. Phys. **82**, 1959–2007 (2010).

[59]D. Xiao, G.-B. Liu, W. Feng, X. Xu, and W. Yao, "Coupled Spin and Valley Physics in Monolayers of MoS_2 and Other Group-VI Dichalcogenides", Phys. Rev. Lett. **108**, 196802 (2012).

[60]K. F. Mak, K. L. McGill, J. Park, and P. L. McEuen, "The valley Hall effect in MoS_2 transistors", Science **344**, 1489–1492 (2014).

[61]J. M. Lu, O. Zheliuk, I. Leermakers, N. F. Q. Yuan, U. Zeitler, K. T. Law, and J. T. Ye, "Evidence for two-dimensional Ising superconductivity in gated MoS_2", Science **350**, 1353–1357 (2015).

[62]X. Xi, Z. Wang, W. Zhao, J.-H. Park, K. T. Law, H. Berger, L. Forro, J. Shan, and K. F. Mak, "Ising pairing in superconducting $NbSe_2$ atomic layers", Nat Phys **12**, Letter, 139–143 (2016).

[63]Y. Saito, Y. Nakamura, M. S. Bahramy, Y. Kohama, J. Ye, Y. Kasahara, Y. Nakagawa, M. Onga, M. Tokunaga, T. Nojima, Y. Yanase, and Y. Iwasa, "Superconductivity protected by spin-valley locking in ion-gated MoS_2", Nat Phys **12**, Letter, 144–149 (2016).

[64]B. T. Zhou, N. F. Q. Yuan, H.-L. Jiang, and K. T. Law, "Ising superconductivity and Majorana fermions in transition-metal dichalcogenides", Phys. Rev. B **93**, 180501 (2016).

[65]N. F. Q. Yuan, K. F. Mak, and K. T. Law, "Possible Topological Superconducting Phases of MoS_2", Phys. Rev. Lett. **113**, 097001 (2014).

[66]J. Zhang, and V. Aji, "Topological Yu-Shiba-Rusinov chain in monolayer transition-metal dichalcogenide superconductors", (2016).

[67]L. P. Gor'kov, and E. I. Rashba, "Superconducting 2D System with Lifted Spin Degeneracy: Mixed Singlet-Triplet State", Phys. Rev. Lett. **87**, 037004 (2001).

[68]R. Roldán, E. Cappelluti, and F. Guinea, "Interactions and superconductivity in heavily doped MoS_2", Phys. Rev. B **88**, 054515 (2013).

[69]J. Fabian, A. Matos-Abiague, C. Ertler, P. Stano, and I. Žutić, "Semiconductor Spintronics", Acta Physica Slovaca **57**, 565–907 (2007).

[70]E. Brown, "Bloch Electrons in a Uniform Magnetic Field", Phys. Rev. **133**, A1038–A1044 (1964).

[71]L. Ballentine, *Quantum Mechanics: A Modern Development* (World Scientific, 1998).